Renewable and Sustainable Energy Reviews 88 (2018) 133–150

Contents lists available at ScienceDirect

Renewable and Sustainable Energy Reviews

journal homepage: www.elsevier.com/locate/rser

Wind turbine noise generation and propagation modeling at DTU Wind Energy: A review

Wei Jun Zhu[a,b,*], Wen Zhong Shen[b], Emre Barlas[b], Franck Bertagnolio[b], Jens Nørkær Sørensen[b]

[a] School of Hydraulic, Energy and Power Engineering, Yangzhou University, Yangzhou 225127, China
[b] Department of Wind Energy, Technical University of Denmark, Lyngby 2800, Denmark

ARTICLE INFO

Keywords:
Wind turbine noise generation
Wind turbine noise propagation
Computational aeroacoustics
Computational fluid dynamics

ABSTRACT

The present review paper provides a comprehensive overview of the research activities on wind turbine aeroacoustics at DTU over the last 20 years, as well as it gives the state-of-the-art of noise prediction models for wind turbines under complex inflow conditions. Various noise generation models developed at DTU are described and analyzed, including models based on the acoustic analogy, flow-acoustics splitting techniques, Amiet's model, and various engineering models. Some of the models are coupled to existing aero-elastic software and computational fluid mechanics models developed at DTU, and implemented in the simulation platform WindSTAR (Wind turbine Simulation Tool for AeRodynamic noise). This simulation platform consists of WindSTAR-Gen, dealing with models for generation of noise and design of low-noise wind turbines, and WindSTAR-Pro, which is developed to handle the modeling of long distance acoustic propagation. As specific features of the WindSTAR-Pro package, the rotation of the noise sources is modeled, the propagation simulations combine the so-called Parabolic Equations (PE) propagation model with numerical flow simulations to take into account effects from wind turbine wakes, atmospheric turbulence and wind shear.

1. Introduction

The recent Paris agreement requires national climate panels to limit the global temperature increase below 1.5 °C, which is a quite challenging task for many countries. Denmark, which is the country with the largest penetration of wind power, had already more than 40% wind power in the electric grid in 2016, and is heading towards 50% by 2020. Due to the vast increase in rotor size and in the number of wind farms, more environmental impact is expected to occur in the future. The newly updated Danish wind turbine noise regulation [1] is very restrictive for both broadband and low frequency wind turbine noise radiation, which in practice may limit the number of new wind farms on land. Unfortunately, energy yield and noise generation are usually two competing factors. Hence, there is an urgent need to develop sophisticated design tools to fulfil the requirements of high power performance and low noise emission in the design of wind turbines and wind farms.

Noise generation from single wind turbines as well as wind farms has its basis in the nature of aerodynamics, caused by the interaction between the incoming turbulent flow and the wind turbine blades. Hence, understanding the mechanisms of airfoil noise generation, demands access to sophisticated numerical tools. The development in High-Performance Computing (HPC) technology provides many possibilities to perform Computational Fluid Dynamics (CFD) and Computational Aero-Acoustics (CAA) simulations of noise generated from rotor blades.

Among the CAA methods, the most accurate way of simulating aerodynamically generated noise is Direct Numerical Simulations (DNS) where both fluid flow and sound are obtained directly by solving the compressible Navier-Stokes (NS) equations. However, due to the high computational costs of using DNS, the acoustic analogy and different hybrid methods are normally used in practice. The acoustic analogy, proposed by Lighthill [2] in the fifties of the last century, is a well-known CAA approach. To generalize the approach, Curle [3] extended the theory by including the influence of static boundaries. Later on, Ffowcs Williams et al. [4,5] extended the theory further by taking into account the influence of moving solid boundaries. The most recent formulations by Farassat et al. [6,7] are well-validated for helicopter rotor noise predictions.

One of the hybrid CAA methods, proposed by Hardin and Pope [8], is based on a flow acoustic splitting technique. Shen and Sørensen [9] improved the theory of Hardin and Pope by changing the basic decomposition of the variables. Some later modifications of the original splitting method are due to Seo and Moon [10] and Ewert and Schröder

* Corresponding author at: School of Hydraulic, Energy and Power Engineering, Yangzhou University, Yangzhou 225127, China.
E-mail addresses: wjzh@dtu.dk, wjzhu@yzu.edu.cn (W.J. Zhu), wzsh@dtu.dk (W.Z. Shen), ebarlas@dtu.dk (E. Barlas), frba@dtu.dk (F. Bertagnolio), jnso@dtu.dk (J.N. Sørensen).

https://doi.org/10.1016/j.rser.2018.02.029
Received 22 December 2016; Received in revised form 22 September 2017; Accepted 27 February 2018
Available online 12 March 2018
1364-0321/

Nomenclature

AL Actuator line
AD Actuator disc
BEM Blade element momentum
BPM Name of the wind turbine noise generation model
BPM-CAA-FLEX Name of the extended wind turbine noise model
CAA Computational aeroacoustics
CFD Computational fluid dynamics
CFL Courant–Friedrichs–Lewy
CNPE The Crank-Nicholson parabolic equation
DNS Direct numerical simulation
DTU Technical University of Denmark
DTU-LN118 The DTU's Low noise airfoil with 18% relative thickness
DRP Dispersion relation preserving
EllipSys3D The DTU in-house flow solver
FFP The fast field program
FFT Fast Fourier transform
FLEX5 The DTU Wind turbine aeroelastic code 5th version
FW-H The Ffowcs-Williams Hawkings's acoustic analogy
GTPE Generalized terrain parabolic equation
GFPE The Greens function parabolic equation method
HAWC2 The DTU's horizontal axis wind turbine simulation code 2nd version
HPC High performance computing
LES Large eddy simulation
LEE Linearized Euler equation
MPI Message passing interface
MW-WAPE Mean-wind wide angle parabolic equation
NREL National renewable energy laboratory
NS Navier-Stokes
PE Parabolic equation
RANS Reynolds averaged Navier-Stokes
SGS Sub-grid-scale
SPL Sound pressure level
TE Trailing edge
TI Turbulence intensity
TNO The noise model named by the organization TNO in Netherlands
TW-WAPE Turbulent-wind wide angle parabolic equation
WAPE Wide angle parabolic equation
WAsP The DTU's wind energy industry-standard software
WindSTAR-Gen Wind turbine simulation tool for aerodynamic noise-Generation
WindSTAR-Pro Wind turbine simulation tool for aerodynamic noise-Propagation

[11], with the aim of reducing the growth of hydrodynamic instabilities. The work carried out by Shen et al. [12–15] was based on the second order time and space discretizations, with the acoustic equations derived directly from the original compressible NS equations. The spitting method was developed further by Zhu et al. [16,17] by implementing high-order low-dispersion schemes [18] to the acoustic equations. In a similar formulation proposed by Bailly and Bogey [19–21], referred to as the Linearized Euler Equations (LEE), the velocity source terms are obtained directly from the compressible NS equations.

Even with today's computer resources, the NS-based CFD and CAA methods are still time consuming for rotor design purposes. Simplified approaches are apparently needed for industrial use in the initial design stage. Based on the general theories, many models were developed from the 1970s to the 1990s. Common for these models is that they consist of different semi-empirical expressions that are derived from the acoustic analogy and fitted to some measured data. In the 1970s, an airfoil turbulent inflow noise model and a trailing edge (TE) noise model were proposed by Amiet [22,23], where the homogeneous turbulent inflow and boundary layer turbulent flow are expressed with sinusoidal wave components and modeled by the von Kármán spectrum, respectively. In parallel with the wind energy development in the 1980s, several other prediction models were proposed [24–29]. Brooks et al. [30] formulated a detailed airfoil self-noise model, which consists of scaling laws for five different aerodynamic noise mechanisms. The airfoil noise model is used in wind turbine rotor noise predictions at DTU [31–33] and NREL [34] where the airfoil self-noise is calculated at each rotor blade segment, the local inflow velocity and angle of attack are obtained from the blade element momentum (BEM) method. In addition to the airfoil self-noise, Lawson's rotor inflow noise model [29] is applied, which takes into account the rotational effects from the inflow noise model of Amiet [22]. The inflow noise basically covers a low frequency noise band in the range 10–160 Hz. Madsen [35] proposed a model that takes into account noise generations at even lower frequencies, which is based on the mechanism of unsteady flows over a wind turbine tower. High frequency noise is often as the result of blade trailing edge noise. The noise mechanism is observed in surface pressure measurements near the TE [36–38] of a wind turbine blade at the DTU test site. At a frequency over 2 kHz, wind turbine noise is normally at a rather low level except for two cases: mechanical noise and trailing edge blunt noise. Mechanical noise originates from the gearbox and bearing systems and has been significantly reduced due to technology development over the last decades. A TE creates tonal noise at a relatively high level. The study of Zhu et al. [33] revealed that blunt TE noise can be reduced to a level well below the overall noise level. The text book of Wagner et al. [39] gives an excellent survey of the different types of noise prediction models for wind turbines. With the available wind turbine noise generation models, noise source reductions have been an important task for aero-acoustic experts. Lutz et al. [40] and Wolf et al. [41] demonstrated that active flow control, such as wall suction, can have a positive effect on the TE noise by controlling the boundary layer thickness along the TE. Some passive flow control devices at the TE are more practical. Passive devices at the TE can be either TE brushes [42–44], TE serrations [45–50], porous TE [51], or even porous TE serrations [52]. The TE serration technique has already been applied for large blades in production by wind turbine and blade manufactories such as Siemens, Gamesa and LM Wind Power. This is discussed more detail in Section 3, where a numerical study of an in-house designed low noise airfoil with TE serration will be presented.

Unluckily, it is not straightforward to move from single wind turbine noise generation to wind farm noise propagation modeling, especially for wind farms built in complex terrain. The ambient turbulence level, terrain geometry, wake interaction between turbines and ground can easily change the noise level and the propagation path over a long distance. Similar to wind resource predictions for wind farm planning, noise evaluations for wind farms should be performed before the wind farm is built, such that inappropriate land-use planning can be avoided. So far, the lack of accurate noise predictions for wind farms becomes challenging for social acceptance of wind power [53]. Social acceptance of wind farms is likely to become one of the most important obstacles for a further development of on-land wind power, as can be seen from studies carried in e.g. Australia [54], Greece [55], France [56], Mexico [57], and many other countries. The studies showed that there is clearly a need to develop advanced wind turbine noise prediction tools to treat these problems in advance. Such a tool should include a wind turbine noise generation model and a long distance propagation model. In most of the previous wind turbine noise propagation studies [58–64], a flat terrain with relatively simplified atmospheric conditions is considered.

Noise propagations in wind turbine wakes were experimentally investigated by Heimann et al. [65], which highlighted the wake effects for wind turbine noise propagations. To consider the atmospheric turbulence effect, Lee et al. [66] applied the Reynolds Averaged NS equations to compute the turbulence field, and combined it with the parabolic wave equation [67] to solve long range noise propagation problems. The study of wind turbine noise propagation over long distances under complex atmospheric condition is a relatively new topic, which will be discussed in the current paper.

The following sections provide a review of the in-house developed noise generation and propagation methods, which form the basis for the code WindSTAR (Wind turbine Simulation Tool for AeRodynamic noise). The topics cover researches from airfoil noise to wind turbine noise generations, including long range propagation under various flow conditions. Due to the need of advanced numerical tools for low noise wind turbine design, as well as low noise wind farm siting and layout design, the developed models should be capable of (1) designing noise-constrained wind turbine airfoils and blades; (2) producing noise maps around the wind farm areas for layout design; (3) providing possible solutions for noise reduction of existing wind turbine or wind farm with acceptable power performance; (4) establishing suitable computational tools for industrial use of full rotor and wind farm optimizations. The paper is organized as follows: Section 2 introduces the wind turbine flow solver, which is the platform of the acoustic solvers; Section 3 discusses various in-house developed wind turbine noise generation models in WindSTAR-Gen (Gen stands for generation); In Section 4, the noise propagation model and the coupling of noise generation and propagation models in WindSTAR-Pro (Pro stands propagation) are discussed, and the detailed wind turbine propagation study is given. A conclusion of the work is presented in Section 5.

2. Wind turbine flow solver

2.1. Governing equations

Flow simulations employing the three-dimensional NS equations are often needed as input to the subsequent CAA computations. For turbulent flow generated noise, different turbulence scales are responsible for the noise generation. In Large Eddy Simulation (LES), the large scales are directly computed, whereas the small scales are modeled by an eddy viscosity based sub-grid-scale (SGS) model. In order to perform LES, two spatial filters are needed. The first filter is equivalent to the finest mesh used in computations and identified by a bar (−). The second filter is denoted as (~) which is the second filter performed on the second finest mesh level. By using these two filters, the incompressible NS equations with velocity-pressure variables read

$$\frac{\partial \overline{U}_i}{\partial t} + \frac{\partial (\overline{U}_i \overline{U}_j)}{\partial x_j} = -\frac{1}{\rho}\frac{\partial \overline{P}}{\partial x_i} + \nu \frac{\partial^2 \overline{U}_i}{\partial x_j^2} + \frac{\partial \tau_{ij}}{\partial x_j}, \tag{1}$$

$$\frac{\partial \overline{U}_i}{\partial x_i} = 0. \tag{2}$$

where U_i,U_j and P are flow velocities and pressure, and the turbulent stresses τ_{ij} in Eq. (1) are expressed as

$$\tau_{ij} = \overline{U_i U_j} - \overline{U}_i \overline{U}_j = (\overline{U_i U_j} - \overline{U}_i \overline{U}_j) - (\overline{U_i' U_j} + \overline{U_i' U}_j) - \overline{U_i' U_j'}. \tag{3}$$

The turbulence fluctuations are defined as $U_i' = U_i - \overline{U}_i$. The turbulent stresses are modeled with an eddy viscosity

$$\tau_{ij} = \nu_t \left(\frac{\partial \overline{U}_i}{\partial x_j} + \frac{\partial \overline{U}_j}{\partial x_i} \right) - \frac{2}{3} k \delta_{ij}. \tag{4}$$

The eddy viscosity is modeled with the mixed scale turbulence model introduced by Ta Phuoc [68]

$$\nu_t = C |\overline{\vec{\omega}}|^{\alpha} k^{(1-\alpha)/2} \Delta^{(1+\alpha)}. \tag{5}$$

The filter size is based on an averaging grid size in three directions such that $\Delta = (\Delta_x \Delta_y \Delta_z)^{1/3}$. The blending coefficient α takes a value in the range between 0 and 1 to balance the vorticity ω and kinetic energy k. Eq. (5) becomes a pure vorticity based model in the case if $\alpha = 1$, such that

$$\nu_t = C |\overline{\vec{\omega}}| \Delta^2, \tag{6}$$

and it becomes the Bardina model [69] in the case if $\alpha = 0$, such that

$$\nu_t = C k^{1/2} \Delta. \tag{7}$$

Assuming similarity between two grid levels, the turbulent kinetic energy can be estimated by using the second filter

$$k = \frac{1}{2}\sum_{j=1}^{3} (U_j - \overline{U}_j)^2 \approx \frac{1}{2}\sum_{j=1}^{3} (\overline{U}_j - \widetilde{\overline{U}}_j)^2, \tag{8}$$

where $\widetilde{\overline{U}}_j$ are the velocities calculated from the second filter, i.e. the velocities are filtered twice.

From the studies on the model parameter [70] it was found that the model generally performs well when the parameter is chosen to be $\alpha = 0.5$.

$$\nu_t = C |\overline{\vec{\omega}}|^{1/2} k^{1/4} \Delta^{3/2}, \tag{9}$$

Where $C = 0.02$ is the model constant. The above mentioned LES model is used in the computations for turbulent airfoil and wind turbine flows.

The filtered NS/LES equations are implemented in the in-house EllipSys3D code, which was developed at the Technical University of Denmark (DTU) [71,72] as a general purpose flow solver. The solver is based on a structured grid topology, with a multi-block and cell-centered finite volume discretization. The NS equations are solved with the pressure-velocity coupling technique where the predictor-corrector method is used. In the predictor step, a second-order backward differentiation scheme is used as time discretization and a second-order central difference scheme is used as spatial discretizations, except that the convective terms are discretized by the QUICK upwinding scheme. In order to avoid numerical oscillations from the velocity-pressure decoupling, the improved Rhie-Chow interpolation [73] is used in the corrector step. Apart from the SIMPLE algorithm, the improved SIMPLEC scheme for collocated grids [74] is also implemented with the advantage that the solution is independent of the relaxation value. The solver is based on a five level multi-grid technique that improves the convergence speed. The EllipSys3D code is programmed with a multi-block topology, and therefore it is parallelized using Message Passing Interface (MPI).

2.2. Applications of LES to airfoil and rotor flows

2.2.1. Airfoil flows

There has been an increased interest of performing turbulent flow CAA/LES computations due to the fast development in computer power and memory. So far, LES is considered the most promising method for handling complex turbulent flow problems. The most applied LES models are based on the works of Smagorinsky [75], Lilly [76], and Deardorff [77], and originally developed for carrying out large-scale weather forecasts. Some other modified LES models were later proposed for flows at smaller turbulent scales. Extensions of the basic Smagorinsky turbulent model were proposed by e.g. Ta Phuoc [68], Sagaut [70], Bardina et al. [69], and many others. Various LES models are available in the in-house EllipSys solver. The model of Ta Phuoc [68] is applied in the current study. As shown in Eq. (9), the eddy viscosity is related to vorticity and turbulent kinetic energy, such that the model is a mixed scale eddy viscosity model. The application of the model is seen in Mary and Sagaut [78] who carried out turbulent flows over a NACA airfoil near stall. From the comprehensive mesh sensitivity study, it was suggested that the mesh resolution expressed in wall unit

should better satisfy the grid size constraints: $\Delta x^+ < 50$, $\Delta y^+ \approx 2$, $\Delta z^+ \approx 20$ where x is in the flow direction, y is in the wall normal direction and z is along the spanwise direction, respectively. Another study by Piomelli and Balaras [79] suggested a range of values as $50 < \Delta x^+ < 150$, $\Delta y^+ \approx 1$, $15 < \Delta z^+ < 40$. For comparison, the criteria used for DNS are: $10 < \Delta x^+ < 20$, $\Delta y^+ \approx 1$, $5 < \Delta z^+ < 10$. With the above-mentioned grid spacing criteria, the limitation of the spanwise spacing is even more critical than in the streamwise direction.

For flows over a NACA 0015 airfoil in a wind tunnel, a detailed comparison of the velocity profile inside the boundary layer between EllipSys/LES and measurements was carried out by Zhu et al. [80]. Good results were also obtained from the EllipSys/LES code in various other studies, including the flow over a bump [81], turbulent jet modeling [82,83], wind turbine rotor simulations [84,85] and turbulent wake interactions [86]. In Fig. 1 an example of the flow field over a NACA 0015 is shown. The chord-based Reynolds number is 1.6×10^5 and the angle of attack changes from 4° to 12°. When the angle of attack increases, the change of flow structure is clearly seen. The separation line moves from a position of about the mid chord towards the leading edge as the angle of attack increases from 4° to 12°. Fig. 2 shows the computed lift and drag data compared with the measurement data of Sheldahl and Klimas [87]. A good agreement is seen for angles of attack below 8°. Some over predictions are observed at large angles of attack where the flow is fully separated from the airfoil suction side surface.

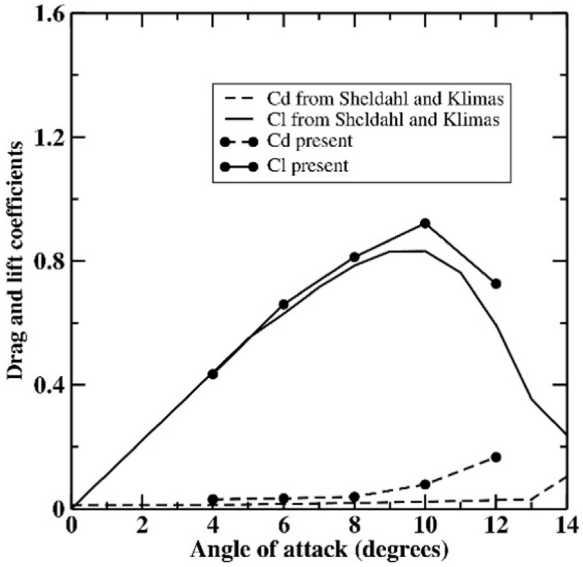

Fig. 2. Comparison of the computed lift and drag coefficients to the experimental data of Sheldahl and Klimas at a Reynolds number of 1.6×10^5 [15].

2.2.2. *Wind turbine flows*

Rotor LES computations using the Actuator Line (AL) technique (the description of the AL technique will be given later in Section 3.5) are used as input to some of the acoustic models, such as the CAA noise generation model and the PE noise propagation model. The purpose of

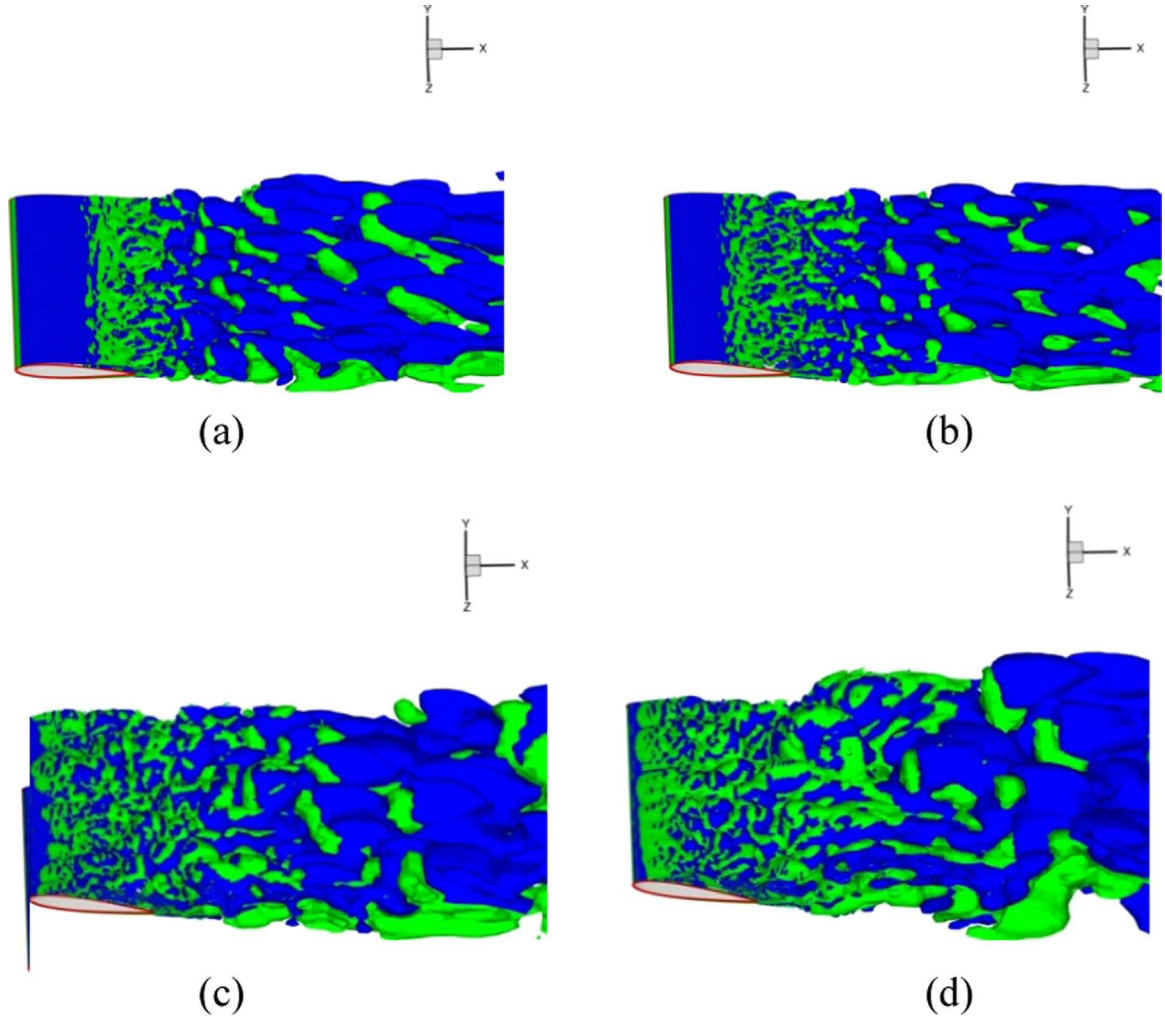

Fig. 1. Spanwise vorticity plots for flows past a NACA 0015 airfoil at a Reynolds number of 1.6×10^5 and angles of attack of (a) 4°, (b) 6°, (c) 10° and (d) 12° [15].

using the LES/AL technique is to provide a detailed unsteady loading on the blades, as well as the structures of the wake behind the rotor. More details about the coupling will be introduced in the later sections. Fig. 3 shows results from LES computations at a relatively high wind speed. The comparisons between simulation and experiment were made in the MexNext project within the framework of IEA task 29. At a wind speed of 24 m/s, the wake results using the original airfoil data (OAD) and modified airfoil data (MAD, corrected for rotational effect etc.) are nearly the same. In the near wake, the axial and tangential velocities agree well with the measured data. In the far wake, the measured data show an earlier wake breakdown, which might be related to the inflow disturbances in the wind tunnel.

3. Wind turbine noise generation models

3.1. Flow acoustic splitting technique

3.1.1. Governing equations

The splitting method is based on the flow and acoustics splitting approach [8,9] and implemented in the EllipSys code as a CAA solver [12–15,17,33]. The compressible NS equations are decomposed into an incompressible flow part and an acoustic perturbation part. The final set of acoustic equations consists of a density equation, a pressure correlation equation and auxiliary correlated velocity fluctuation equations

$$\frac{\partial \rho^*}{\partial t} + \frac{\partial f_i}{\partial x_i} = 0, \tag{10}$$

$$\frac{\partial p^*}{\partial t} - c^2 \frac{\partial \rho^*}{\partial t} = -\frac{\partial \overline{P}}{\partial t}, \tag{11}$$

$$\frac{\partial f_i}{\partial t} + \frac{\partial}{\partial x_j}\left[f_i(\overline{U}_j + u_j^*) + \rho_0 \overline{U}_i u_j^* + \left(p^* + \frac{2}{3}\rho^* k\right)\delta_{ij}\right] = \frac{\partial}{\partial x_j}\left[\rho^* \nu_t \left(\frac{\partial \overline{U}_i}{\partial x_j} + \frac{\partial \overline{U}_j}{\partial x_i}\right)\right], \tag{12}$$

The unknowns with a superscript (*) indicate acoustic variables and the capital letters $\overline{U}_i$, $\overline{U}_j$ and P are the resolved incompressible flow variables obtained from Eq. (1). The auxiliary variables are defined as $f_i = \rho u_i^* + \rho^* \overline{U}_i$. The equation system is closed with a speed of sound equation that is valid for ideal gases,

$$c^2 = \frac{\gamma(\overline{P} + p^*)}{\rho_0 + \rho^*}. \tag{13}$$

Acoustic computations may start at any time. The incompressible flow parameters form the input to the acoustic equations. The flow and acoustic simulations can have different meshes and different time-steps determined from their CFL (Courant–Friedrichs–Lewy) numbers, which can greatly accelerate the computations. In the following CAA calculations, the incompressible NS equations are always solved by the second-order finite volume EllipSys code, but the acoustic equations have the option to be solved with high-order wavenumber optimized schemes, ranging from 2nd-order to 12th-order accuracy schemes [17].

3.1.2. Applications of the splitting method

As mentioned earlier, a high mesh resolution is often required to solve waves with a small wavelength. It is thus difficult to carry out full LES wind turbine simulations with current computational resources. For wind turbine flows, the sound speed is typically 3–4 times faster than the tip speed of a large wind turbine, thus the acoustic time step is limited to at least 3–4 times smaller than the one used in flow simulations if a similar mesh resolution is used for both flow and acoustics. Therefore, many CAA/LES, DNS studies are aimed at turbulent induced airfoil noise [88–92]. To reduce the dispersion error on a given mesh, high-order finite difference or high-order compact schemes are often applied in CAA. The Dispersion-Relation-Preserving (DRP) finite difference scheme [18] was derived for such purpose. Instead of minimizing dissipation errors, the new schemes are optimized for dispersion errors. Based on the method of Tam and Webb [18], various optimized central difference schemes [17,93,94], upwind finite difference schemes [95,96] and backward schemes for boundaries [93,97] were derived and applied. Both optimized finite difference schemes and compact schemes are implemented in the aeroacoustic solver up to 12th-order. The optimization of compact schemes is based on the original compact scheme of Lele [98]. The derivation of spectral-like compact schemes was given by Kim et al. [99] and Visbal et al. [100]. The use of high-order compact boundary schemes [101] is an issue that causes numerical instabilities which was studied by Carpenter et al. [102].

Table 1 gives an overview of the standard central difference schemes compared with the optimized ones. The table lists the maximum resolvable wavenumbers $\overline{\alpha}\Delta x$ under three dispersion errors: $\varepsilon = 0.1$, $\varepsilon = 0.01$ and $\varepsilon = 0.001$. For a given accuracy of $\varepsilon = 0.001$, using a

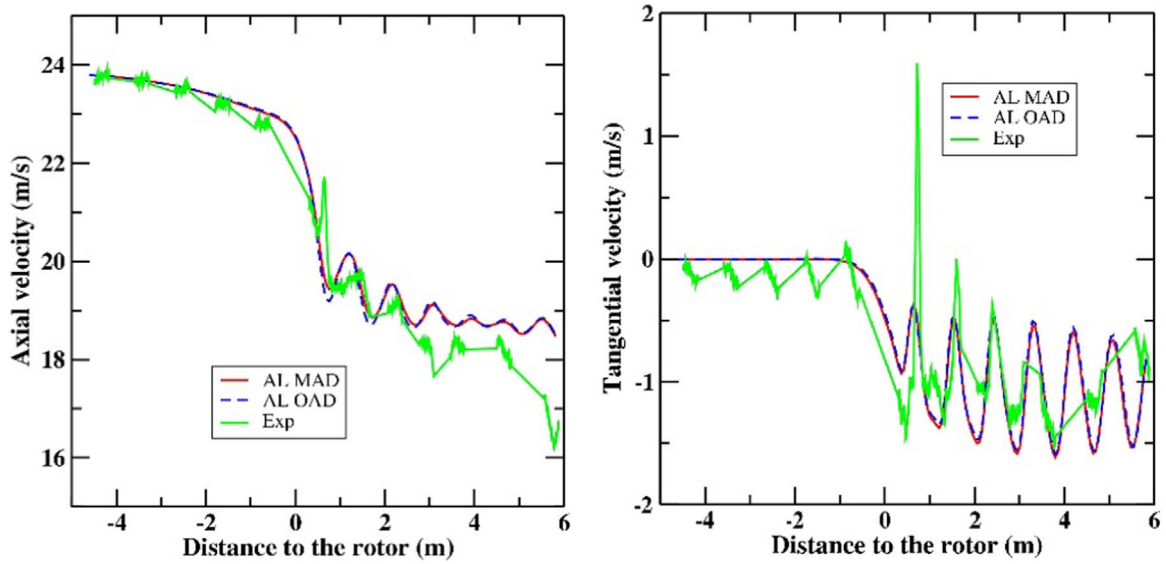

Fig. 3. Axial and tangential velocity along the line in the axial direction at r = 1.848 m and 9 o'clock for the flow at a wind speed of 24 m/s, a pitch angle of − 2.3° and a rotor speed of 424.5 rpm [84].

Table 1
Maximum resolvable wave number $\bar{\alpha}\Delta x$ of the finite difference schemes.

Schemes	$\varepsilon = 0.1$	$\varepsilon = 0.01$	$\varepsilon = 0.001$
(a) 2nd original	0.707	0.243	0.075
(b) 4th original	1.254	0.743	0.417
(c) 6th original	1.536	1.089	0.731
(d) 4th optimized	1.717	1.509	1.431
(e) 6th optimized	1.834	1.605	1.481
(f) 8th optimized	1.921	1.695	1.525
(g) 10th optimized	1.990	1.776	1.576
(h) 12th optimized	2.045	1.848	1.629
(i) 14th optimized	2.091	1.913	1.682

8th-order DRP scheme instead of a 2nd-order central difference scheme yields a grid size reduction of $(\bar{\alpha}\Delta x)^{DRP8}_{\max}/(\bar{\alpha}\Delta x)^{CDS2}_{\max} = 1.525/0.075 \approx 20$.

Fig. 4 shows the flow and acoustic results over a NACA airfoil at a Reynolds number of 10^5, an angle of attack of 5° and a Mach number of 0.2. The numerical domain extends 25 chord-lengths in the radial direction. A structured body-fitted curvilinear mesh is used in this study. The grid is stretched exponentially towards the outer boundary with the first wall cell size below 10^{-5} of the chord length. The dipole-like acoustic waves are generated at the airfoil TE and travel outwards. The noise amplitude is much higher in the direction normal to the airfoil chord.

Time history signals of the acoustic pressure are saved at each time iteration for purpose of making Fourier analyses. The noise spectra obtained at an angle of attack of 6.7° are compared with acoustic measurements [30]. As shown in Fig. 5, the 1/3-octave band sound pressure spectra are compared at several free stream velocities: from 31.7 m/s to 71.3 m/s. The results show that the level of airfoil noise is proportional to the incoming wind speed. Despite of the laminar boundary layer instability, airfoil tonal noise [103–105] from high Reynolds number flows usually generates stronger noise sources due to larger flow disturbances at the TE. By comparing the noise spectra, it is also seen that the spectrum shifts towards the higher frequency region while the wind speed increases.

3.2. Acoustic analogy

3.2.1. Governing equations

In this section, the integrated formulation proposed by Farassat [6] is applied. The formulation is a solution to the Ffowcs Williams-Hawkings (FW-H) equation with the surface noise sources, when the surface moves at a subsonic speed. This formulation has been successfully used for helicopter rotor and propeller noise predictions. The thickness and loading noise sound pressure fluctuations are written in function of source terms at the retarded time as

$$4\pi p'_T(\vec{x}, t) = \frac{\partial}{\partial t}\int_{f=0}\left[\frac{\rho_0 v_n}{r(1-M_r)}\right]_{ret} dS \tag{14}$$

$$4\pi p'_L(\vec{x}, t) = \frac{1}{c}\frac{\partial}{\partial t}\int_{f=0}\left[\frac{p\cos\theta}{r(1-M_r)}\right]_{ret} dS + \int_{f=0}\left[\frac{p\cos\theta}{r^2(1-M_r)}\right]_{ret} dS \tag{15}$$

where p'_T and p'_L represent thickness and loading noise, respectively. Again, a flow solution is required for solving the acoustic integrals. The flow parameters include the wall normal velocity component v_n, the instantaneous pressure on the solid wall surface, p. Other inputs are the Mach number of the noise source in the radiation direction, M_r, the distance between source and receiver, r, the angle between the radiation direction and the local wall normal direction, θ. Fig. 6 shows a sketch of an airfoil where dS indicates one of the typical wall element that is integrated over the entire airfoil surface. It is obvious that the angle θ will contribute to the noise directivity. The right hand sides of Eqs. (14) and (15) are the integrations of time history variables obtained from flow calculations. The acoustic solver may run together with the NS solver or the acoustic solver starts when the flow-field is fully established. For the retarded time approach, the flow data are recoded in advance with a period of r/c in order to calculate the time derivatives at the emission time. The weak point of the integral acoustic equations is to predict the acoustic diffraction phenomenon due to body obstacles.

3.2.2. Applications of acoustic analogy

The airfoil to be investigated is the DTU-LN118 airfoil [106]. The surface mesh and the side view of the volume mesh are shown in Fig. 7. The baseline DTU-LN118 airfoil is attached with serrations at the trailing edge. The wind speed used in the simulation is 45 m/s, the airfoil chord is 0.6 m, the serration length is 16.7% of the baseline airfoil chord and the serration wave length is 50% of the serration length. The surface pressure at an angle of attack of 6° is extracted from the LES results. In Fig. 8, the time averaged surface pressure distribution from LES is first compared with the wind tunnel experiment. The results show very small differences with the experiment for either the

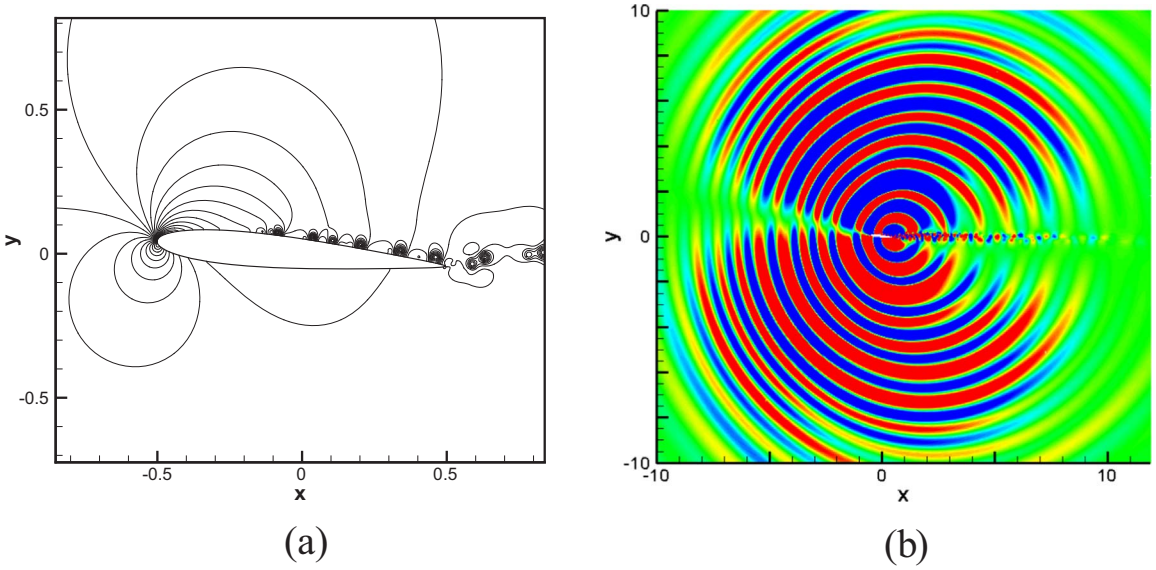

Fig. 4. Example of (a) incompressible pressure contours and (b) sound pressure field for the flow past a NACA 0012 airfoil at $Re = 100{,}000$, M = 0.2 and $\alpha = 5^{\circ}$ [17].

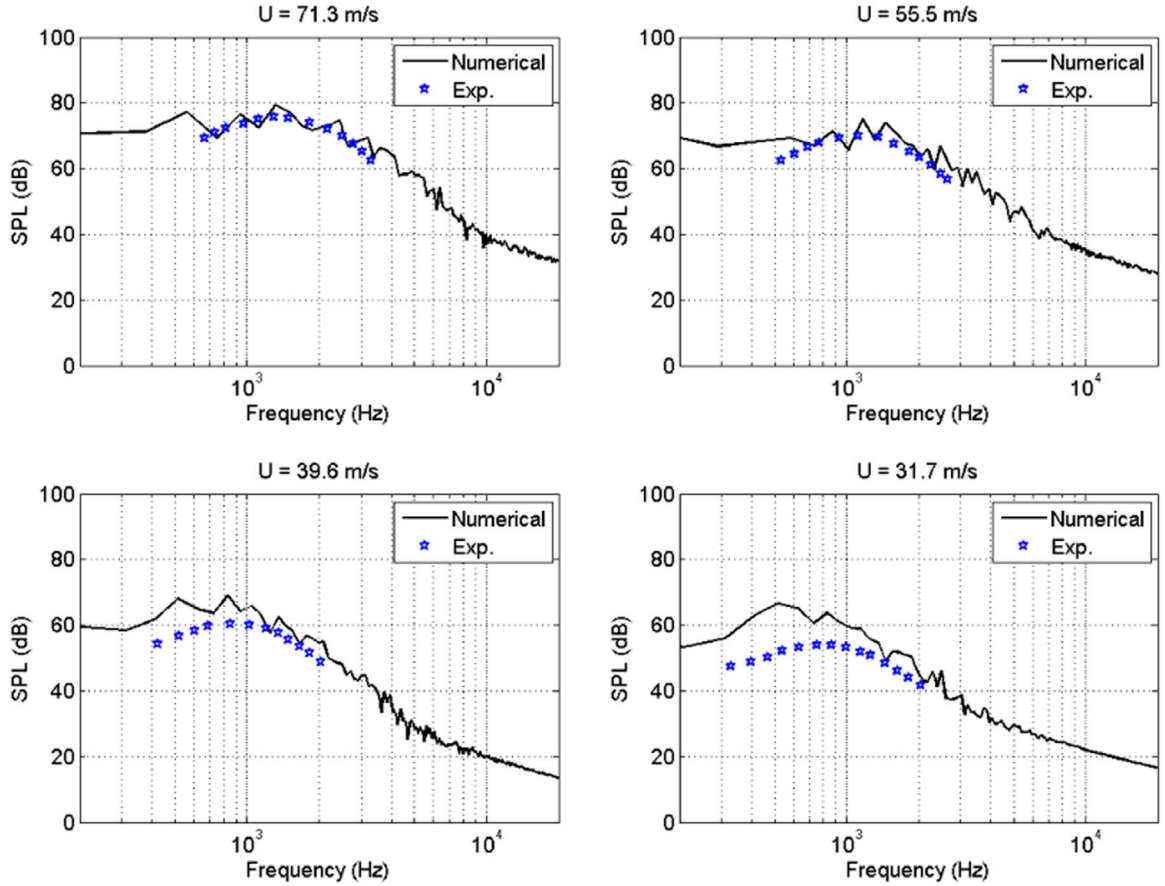

Fig. 5. Comparison of 1/3 octave band noise spectra at an angle of attack of 6.7° [17].

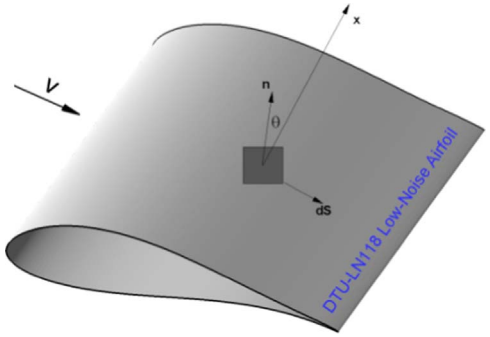

Fig. 6. Sketch of an airfoil surface.

original DTU-LN118 airfoil, or the airfoil with serration. A small difference is observed near the trailing edge. The results indicate that the serration does not give big influences on the airfoil aerodynamics. On the right hand side of Fig. 8, the measured and simulated noise spectra are compared and good agreements are seen. The general trend from both results confirms the effectiveness of the trailing edge serration. The noise reduction mechanism is caused by the redistribution of the surface pressure distribution at TE [107] that decreases the loading noise as expressed in Eq. (15). In the previous work by Zhu et al. [107–109] it was shown that the detailed noise reduction at the TE depends on many parameters, such as angle of attack, flap angle of the serration, wavelength of the serration, amplitude of the serration, etc. Although different combinations of these parameters yield in different noise levels, noise reductions are observed in most of the simulation cases.

3.3. Amiet's model

3.3.1. Governing equations

Amiet's model consists of a TE noise model and a turbulent inflow noise model. The derivation of Amiet's model is based on a simplified airfoil geometry. The model considers a flat plate at zero angle of attack and zero thickness [23,110]. The calculation of TE noise is related to the incident wall pressure field that passes the trailing edge. The wall pressure spectrum is split by Fourier analysis into wave numbers which are the chord-wise wavenumber component K_x and the spanwise wavenumber component K_y [111]. The wall pressure fluctuation corresponding to the wavenumber $\boldsymbol{K} = (K_x, K_y)$ generates a farfield acoustic pressure spectrum which can be written by the radiation integral

$$S_{pp,TE}(\vec{x}, \omega) = \left(\frac{\omega c x_3}{4\pi c_0 S_0^2}\right)^2 \frac{L}{2} \left|\Upsilon_{TE}\left(\frac{\omega}{U}, \frac{k x_2}{S_0}\right)\right|^2 \Phi_{pp}(\omega) l_y\left(\omega, \frac{k x_2}{S_0}\right) \tag{16}$$

where (x_1, x_2, x_3) are the observer coordinates and (y_1, y_2, y_3) are the source coordinates at retarded time, x_1 is in the chordwise direction, x_2 is along the spanwise direction and x_3 is in the wall normal direction; $\beta_0 = (1\text{-}M^2)^{1/2}$ is a Mach number correction, L is the airfoil span, c is the chord length, Υ_{TE} is the transfer function for trailing edge noise [111], Φ_{pp} is the wall pressure spectrum which uses Goody's zero pressure gradient model [112] for the pressure side and Rozenberg et al.'s adverse pressure gradient model [113] for the suction side, l_y is the spanwise correlation length, and $S_0 = \sqrt{x_1^2 + \beta_0^2(x_2^2 + x_3^2)}$. The calculation of power spectral density can be carried out in the frequency domain by integrating all the contributions for a single frequency. Amiet's model for turbulent inflow noise is expressed in the similar format such that the far-field acoustic power spectral density is written as:

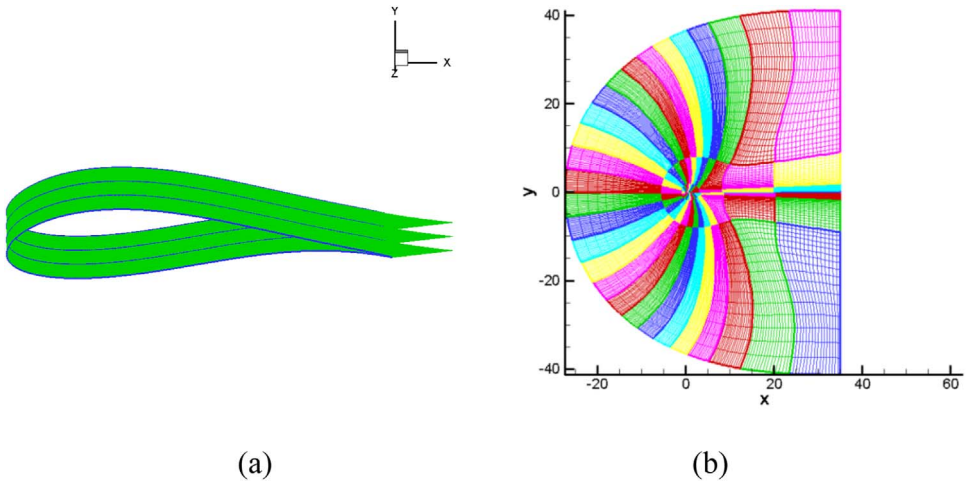

Fig. 7. (a) Wall surface mesh; (b) volume mesh side view.

$$S_{pp,Inf}(\vec{x}, \omega) = \left(\frac{\rho_0 \omega c x_3}{2\pi c_0 S_0^2}\right)^2 \pi U \frac{L}{2} \Phi_{ww}\left(\frac{\omega}{U}, \frac{k x_2}{S_0}\right) \left|\Upsilon_{Inf}\left(x_1, \frac{\omega}{U}, \frac{k x_2}{S_0}\right)\right|^2 \quad (17)$$

where Υ_{Inf} is the transfer function for the inflow noise [111].

The turbulence fluctuation spectrum is defined by the Von Karman spectrum model such that

$$\Phi_{ww}(K_x, K_y) = \frac{4}{9\pi} \frac{\overline{\sigma}_u^2}{K_e^2} \frac{\hat{K}_x^2 + \hat{K}_y^2}{(1 + \hat{K}_x^2 + \hat{K}_y^2)^{7/3}} \quad (18)$$

where $\hat{K} = K/K_e$ and $\overline{\sigma}_u$ is the standard deviation of the turbulent velocity fluctuation, such that the turbulence intensity is given as $TI = \overline{\sigma}_u/U$; K_e is a function of the integral turbulence length scale Λ,

$$K_e = \frac{\sqrt{\pi}}{\Lambda} \frac{\Gamma(5/6)}{\Gamma(1/3)} \quad (19)$$

3.3.2. Applications of Amiet's model

There have been several studies using Amiet's model for wind turbine noise prediction [114–116] which illustrated relatively good results. Here Amiet's model is used to predict noise generation from the NordTank 500 kW wind turbine with a rotor diameter of 41.4 m, located at DTU's Risø Campus. The blade consists of 4 airfoils section geometries. Section 1: FFA-W3-241 airfoil at $r = 10$ m; Section 2: FFA-W3-211 airfoil at $r = 11$ m; Section 3: NACA $63_3$418 airfoil at $r = 12.5$ m; Section 4: NACA$63_3$415 airfoil at $r = 19.5$ m. For the four sections, the airfoil shape, Reynolds number, Mach number and flow angle of attack are known as input, where the angle of attack is computed with a standard BEM code. A mean wind speed of 8.5 m/s is used for comparison. The nearfield noise measurements were performed on the full scale NordTank 500 kW wind turbine [117] with 8 microphones placed on the ground around the wind turbine. Microphone data at selected positions are compared with results from Amiet's model. The rotor total noise is obtained by summing up all noise elements at each blade section for all three blades. The section noise level is obtained from the TE noise on the suction side and pressure side, and the inflow noise, such as

$$SPL_{section} = 10\log_{10}(10^{0.1SPLs} + 10^{0.1SPLp} + 10^{0.1SPLinflow}) \quad (20)$$

Fig. 9 shows the results obtained from both measurements and predictions. Two different wall surface pressure models are used to distinguish the model sensitivity. The 'Amiet's model A' applied the Rozenberg adverse pressure gradient model, and Goody's zero pressure gradient model is used in the 'Amiet's model B'. The model generally performs well in the whole frequency range. The measured background noise is low enough except at frequencies lower than 20 Hz. At such low frequencies, there are uncertainties both coming from the modeling side and the measurement side where the background noise has larger variability. As seen from the current results, the different wall surface pressure models of Amiet's model only leads to very little differences.

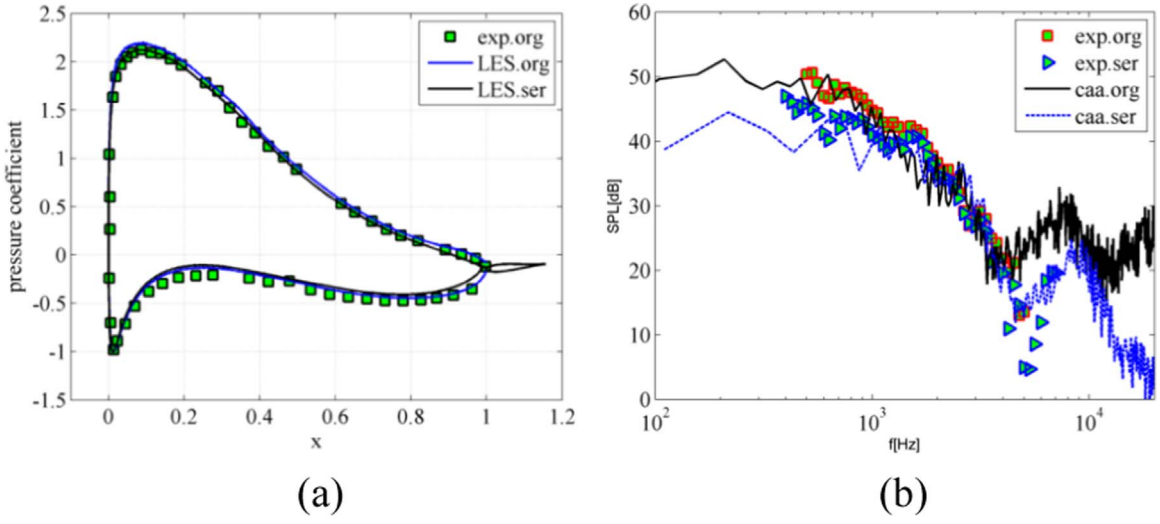

Fig. 8. Comparisons of: (a) surface pressure and (b) noise spectra with measurements at an angle of attack of 6° [107].

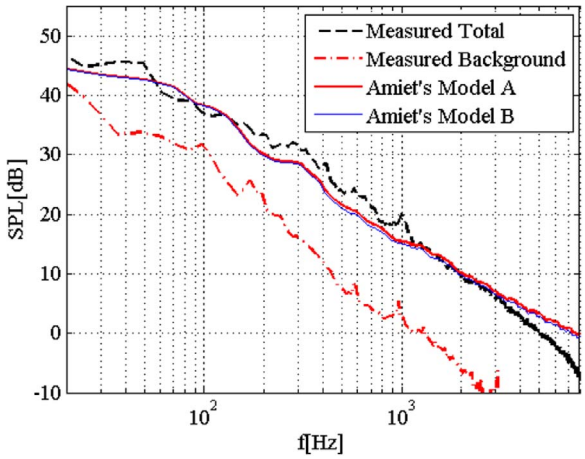

Fig. 9. Predictions using Amiet's model and compared with DTU field measurements at a free-stream velocity of 10 m/s.

3.4. Improved wall pressure spectrum model

3.4.1. Governing equations

This model is named as HAWC2-Noise model. The original so-called TNO model [118] has been improved at DTU Wind Energy through several studies [119–121]. The original form suffers from deficiencies, especially at high flow angles of attack. The improved TNO model reads,

$$\Phi_{pp}(k_{||}, \omega) = 4\rho_0^2 \frac{k_1^2}{k_1^2 + k_3^2} \int_0^{\delta_{BL}} 2L_2(y) \left(\frac{\partial U_1}{\partial y}(y)\right)^2 \times \overline{u_2^2}(y) \widetilde{\Phi}_{22}(k_{||}, \Lambda) \Phi_m(\omega - U_c(y)k_1) e^{-2k_{||}y} dy \tag{21}$$

where $k_{||} = (k_1, k_3)$ is the norm of the wavenumber vector spanning the plane that is parallel to wall, δ_{BL} is the boundary layer thickness, L_2 is the vertical correlation length characterizing the vertical turbulent velocity component u_2, $\overline{u_2^2}$ denotes its mean squared value of the vertical velocity fluctuation, U_1 is the mean velocity in the stream-wise direction, $\widetilde{\Phi}_{22}$ is the normalized spectrum of the vertical velocity fluctuation which is integrated along k_2, and Φ_m is the moving axis spectrum that describes the distorted $\widetilde{\Phi}_{22}$ term by the generation and destruction of turbulent eddies at TE. The convection velocity is approximately 70% of the mean stream-wise velocity. In [122], it is proposed that the double-integral originating for the cross-correlation between boundary layer sheets above the trailing edge is kept in the numerical integration (instead of the simplified approach of formula (21), where turbulence is assumed de-correlated between these boundary layer sheets). This helps further improving the TNO model at lower frequencies where the large associated vortices indeed extend over larger distances across the airfoil turbulent boundary layer. More details about the parameter settings of the TNO model are referred to the previous studies [120–122].

Apart from the TNO trailing edge noise model, the stall-noise model is developed separately. The stall-noise spectrum is developed from Amiet's farfield noise formulation [110] of the adapted TE noise version by Bertagnolio et al. [123,124]. In order to model wind turbine rotor aerodynamically generated noise, the in-house developed code HAWC2 [125] is coupled with the TNO model as well as the stall noise model. The relative inflow velocity and local angle of attack are inputs from the HAWC2 code. By knowing the local angle of attack at blade sections, the HAWC2-Noise model automatically switches between TE noise and stall noise mechanisms. To reduce the simulation time, the required boundary layer parameters at the blade surface are pre-generated and saved as a look-up table.

3.4.2. Applications of the improved wall pressure spectrum model

We use the same noise measurement data of the NordTank 500 kW wind turbine [126] to compare the HAWC2-Noise model. In Fig. 10, the wind turbine noise measured by microphones located downwind of the rotor is compared with the current prediction model. The inflow noise model of Amiet is also included for fair comparison. The model prediction is based on the unsteady HAWC2 calculation, and therefore the results are finally averaged over time. There is a quite good agreement between the experiment and model prediction. In the plots, the spectra of measured background noise are also displayed. Using the improved TNO model and the unsteady HAWC2 model, the predictions are slightly better than Amiet's model.

3.5. Coupled computational aeroacoustic and actuator line model

This section introduces a hybrid method [127,128] that combines a semi-empirical noise model with an advanced CAA method. The acoustic simulations and LES/AL simulations are performed at the same time. In the case of flexible blades, the aero-elastic code FLEX5 is an optional build-in tool. This model is named as BPM -CAA-AL-FLEX5 method.

3.5.1. Governing equations

3.5.1.1. The classic BPM model. In the BPM model, the modeling of turbulent inflow noise is based on Lawson [29]

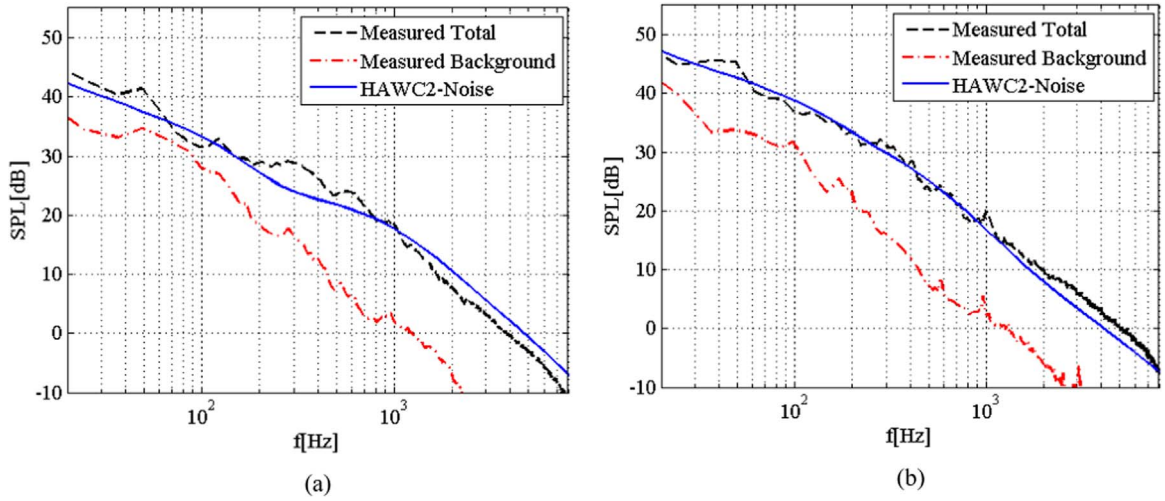

Fig. 10. Predictions using the HAWC2-Noise model and compared with DTU field measurements: (a) at 5 m/s free-stream velocity; (b) at 10 m/s free-stream velocity.

$$\mathrm{SPL}_{inflow} = 10log_{10}\left[D\rho^2 c_0^2 L\frac{\Delta l}{r^2}M^3 I^2 \hat{k}^3 (1+\hat{k}^2)^{-7/3}\right] + C. \quad (22)$$

where SPL is sound pressure level, D is the sound directivity, ρ is the air density, c_0 is sound speed, L is the typical atmospheric turbulence length scale, Δl is the airfoil section semi-span, C is the constant, M denotes the Mach number, $\hat{k}$ is the normalized wavenumber and I is the turbulence intensity. The rotor self-noise calculation is based on the 2D airfoil self-noise model [30]. A steady BEM method is often combined with the airfoil self-noise model which consists of scaling laws for several noise mechanisms. The general form of the airfoil self-model reads,

$$\mathrm{SPL} = 10log_{10}\left(\frac{\delta M^n l D}{r^2}\right) + G_1(St) + G_2(Re) + G_3(\delta) + C. \quad (23)$$

In Eq. (23), it is shown that the airfoil noise is related to a thickness parameter δ, either relating to the boundary layer thickness or blunt TE thickness. The length parameter l represents either length of the airfoil span or length of the blade tip. The other functions, G_1, G_2 and G_3 are related to the Strouhal number, Reynolds number and thickness parameter. The major self-noise mechanisms are depicted in Fig. 11, where TE noise, TE blunt noise, stall noise and tip noise are individually shown.

The wind turbine noise prediction model directly applies the airfoil noise model to the rotating wind turbine blades [31]. The total wind turbine aerodynamic noise is summed up from all the blade elements such as

$$SPL_{total} = 10log_{10}\left(\sum_i^n 10^{0.1SPL^i_{total}}\right) \quad (24)$$

where the total noise is summed with n blade elements and SPL^i_{total} is the total noise from airfoil element i.

3.5.1.2. Actuator line model. The development of the BPM noise prediction tool requires rotor aerodynamic computations as the basic input to the model. The most popular method used for this purpose is the BEM method that directly computes the local velocity and angle of attack at the blade elements. A new approach, using the CFD based Actuator Line (AL) technique [129] is introduced by Debertshäuser et al. [127,128]. The AL technique breaks the limit of the BEM method and the outputs from an aerodynamic simulation are the time dependent, fluctuating flow field. The complex flow conditions can thus be modeled, such as turbulent inflow, wind shear and yaw etc. The time dependent flow parameters extracted from CFD computations are fed to the BPM model. The approach to compute the flowfield over wind turbine blades is done by adding a volume body force to the momentum equation

$$\frac{\partial U_i}{\partial t} + \frac{\partial (U_i U_j)}{\partial x_j} = -\frac{1}{\rho_0}\frac{\partial P}{\partial x_i} + \nu\frac{\partial^2 U_i}{\partial x_j^2} + \boldsymbol{f}, \quad (25)$$

$$\boldsymbol{f} = \frac{1}{2}\rho V_{rel}^2 c(C_L, C_D). \quad (26)$$

The force $\boldsymbol{f}$ is computed iteratively with the blade element approach combined with tabulated airfoil lift and drag data such as C_L and C_D. As shown in Fig. 12, the elements of the rotating blades are represented with a body force. At each time step, the EllipSys3D flow solver gives a velocity field. The relative velocity V_{rel} at each blade segment is calculated by identifying the index of the blade position at the current time instant. Fig. 12(b) shows the vortex field generated from the blade tip and root, which is created by the rotating volume force. Another advantage of the AL approach is to couple with the in-house developed aeroelastic code FLEX5 that handles more complex structural deformation and thus influences noise generation to a certain degree.

3.5.2. Applications of the coupled model

Fig. 13(a) illustrates the user interface of the BPM noise prediction tool. The input of blade geometry as well as airfoil data is required by the BEM model. Turbulence length scale and turbulence intensity are inputs to the inflow noise model. TE geometry details, such as bluntness and serration size are applied for the purpose of providing more specific modeling of the geometry. The A-weighted sound pressure spectra are calculated and compared with measurements at wind speeds of 6, 8, 10 m/s. The model is seen to be in good agreement with the experiment, especially at wind speeds of 8 and 10 m/s.

The wind turbine noise generation under atmospheric turbulence and wind shear conditions becomes more difficult. The modeling approach is shown in Fig. 14 where *Step1* contains the LES/AL flow simulation and *Step2* contains the CAA splitting method and the BPM hybrid models. The low frequency noise created from the atmospheric turbulence and wind shear is captured by the CAA model using the splitting technique. To apply the CAA approach only for low frequency calculations greatly saves the computational time. The higher frequency component is calculated with the BPM model using the flow input obtained via LES. The time dependent angle of attack at each blade element is computed from the AL technique. In Fig. 15 the stream-wise velocity field at a wind speed of 10 m/s is shown. The wind turbine is located at Z = 5 R, and Y = 1.8 R. The atmospheric turbulence is introduced at Z = − 1 R and thus influences the incoming flow facing the wind turbine, as well as the wake development. In particular, the turbulence influences the local angle of attack and local relative velocity used for the BPM noise calculation, and the noise radiation in the computational domain. The noise radiation is governed by Eqs. (10)–(12).

At a wind speed of 10 m/s, the wind turbine generated aerodynamic noise field is seen in Fig. 16. As shown in the figure, there is a high level of sound pressure generated at the rotor position. The propagation of wind turbine noise is influenced by the atmospheric turbulence as well as by the wake turbulence. More details about the wind turbine noise propagation will be introduced later in this paper. As a result of the time history sound pressure, Fig. 17 contains the overall sound pressure level recorded during a time period of about two minutes at three wind speeds. The fluctuation of the sound pressure level is due to the inflow turbulence, wake and wind shear effects.

3.6. Summary of the wind turbine noise generation models

In this section, the in-house developed wind turbine noise generation models are introduced with both theory and examples. These methods are: (1) Flow/acoustic splitting method, (2) Acoustic analogy, (3) Amiet's model, (4) HAWC2-Noise, (5) classic BPM, and (6) BPM-CAA-AL-FLEX5 method. Ranking the models in model accuracy, complexity and computational cost we have the decreasing order of (1), (6),

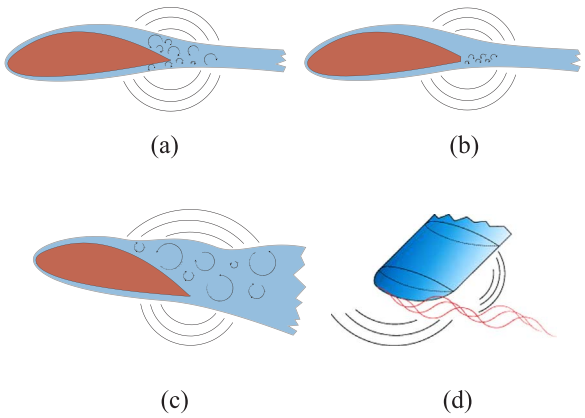

Fig. 11. Wind turbine blade self-noise mechanisms.

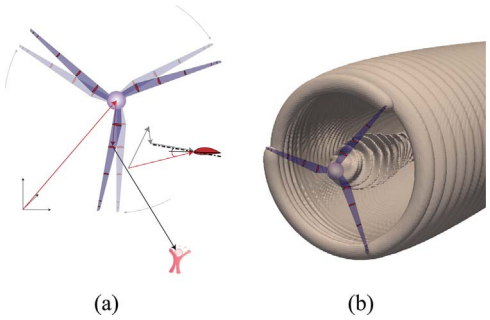

(a) (b)

Fig. 12. (a) Rotating blades are divided into elements; (b) vortex wake behind the rotor.

(2), (4), (3), (5). The same order applies when considering model uncertainties. Methods (1) and (6) involves LES and CAA computations at the same time duration. Particularly, LES requires a fine mesh near the solid boundary and the mesh density for CAA is more critical over a large domain of interest [17,18]. For the time discretization, the difference between the flow speed and sound speed leads to a smaller time step used for CAA than for CFD. Although there are certain limitations of the splitting approach, it is still one of the most accurate approaches to study near-field noise generations. Method (2) still requires an unsteady CFD simulation until the flow is stabilized. However, the acoustic computation is only performed at the solid surface by integrating the fluctuating pressure and velocities around the wall region. Thus there is no limitation of spatial and time resolution while using acoustic analogy. Methods (3) and (4) belong to the same group which does not necessarily require unsteady CFD computations. Despite the analytical methods, CFD computations of the trailing edge boundary layer thickness and fluctuating wall pressure are also applied to improve the model accuracy. The computational time of Method (5) is typically in the order of seconds, which also depends on whether steady or unsteady BEM is applied. Since it is a semi-empirical method, it has the largest uncertainties. The accuracy of airfoil data, the detailed TE boundary layer thickness, and the model of inflow condition make it less accurate. User's experience of selecting a model also has an impact to the output results. Due to the high efficiency, the BPM method is widely used in industrial applications, as well as in low noise wind turbine design [130].

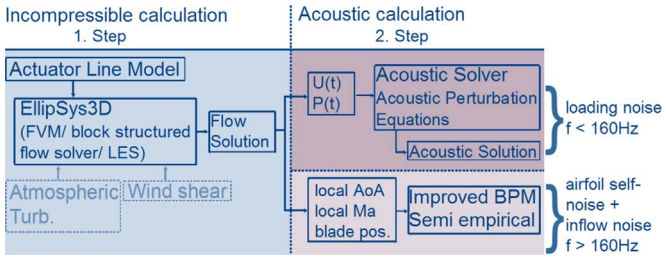

Fig. 14. Flow chart of the coupled model.

4. Modeling of the wind turbine noise propagation

The models described in this section form the basis of the WindSTAR-Pro package. The model is a combination of several sub-models: wind turbine noise generation models, turbulent flow models, noise source models and a noise propagation model [131–134].

4.1. Methodology of the propagation model

Various outdoor sound propagation modeling techniques are available that can be adopted for predicting wind turbine and wind farm noise propagations, see Berengier et al. [135] for a brief review. Due to the wind turbine noise source characteristics, most of the methods cannot be directly used as a wind turbine noise propagation tool. For far field noise propagations, we choose to apply the Parabolic Equation (PE) model as a compromise between numerical accuracy and computational effort. The PE method is a solution of the wave equation using the approximation of a harmonic wave propagation with a finite angle for forward or backward propagations. The solution of each PE simulation yields a steady solution at each frequency. For rotor noise propagation cases, if a time dependent solution is desired, multiple PE simulations can be carried out successively in order to capture the SPL time evolution.

Following the notations in Blanc-Benon et al. [136], the PE methods can be divided into two groups: scalar PE and vector PE. The scalar PE is the conventional approach where the moving atmosphere is represented by a hypothetical frozen medium with a fixed effective sound speed $c_{eff} = c+v_x$ where v_x is the wind velocity component along the direction of propagation between source and receiver. For the vector PE, the vector properties of the velocity field are maintained, which can be obtained from a flow simulation. Thus the propagation equation

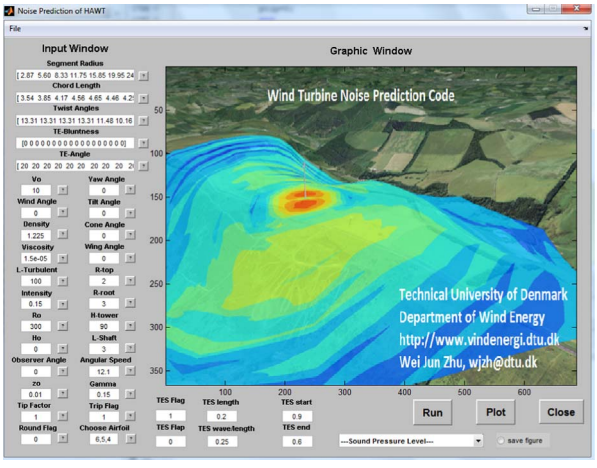

(a)

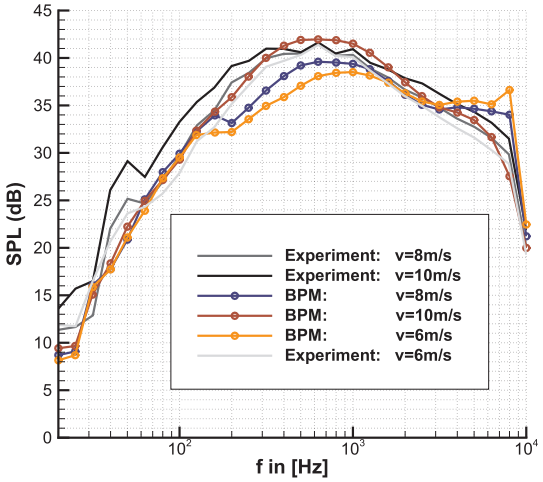

(b)

Fig. 13. (a) User interface of the noise prediction model. (b) Predictions using the BPM model and compared with DTU field experiments at free-stream wind speeds of 6 m/s, 8 m/s and 10 m/s.

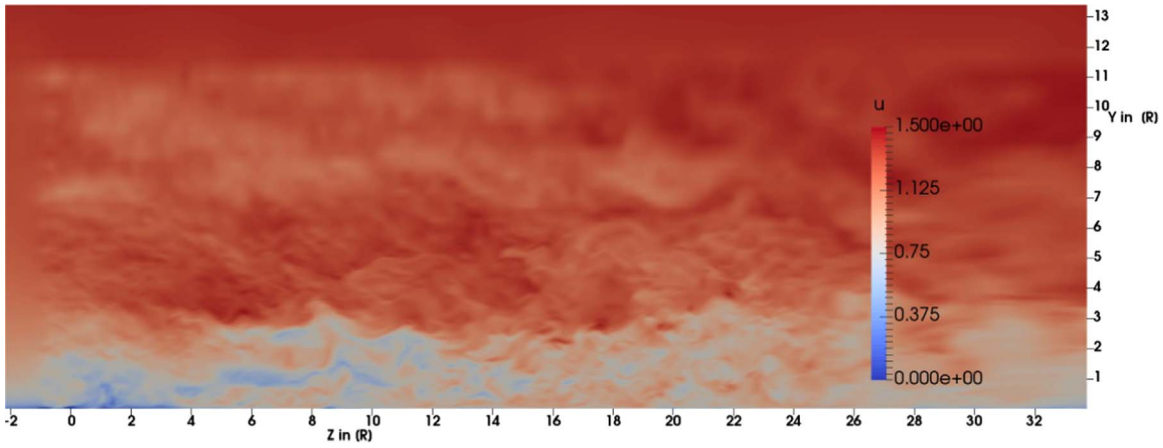

Fig. 15. Normalized steam-wise velocity out of the actuator line method; rotor is positioned at z = 5 R and y = 1.8 R.

contains new terms. The scalar PE method is expected to perform well when the source and receiver are close to the ground because the sound propagation direction is nearly horizontal and the scattering angle (angle between the sound wave and a wave scattered by turbulence) does not exceed a certain limit. For both methods, the derivation can be carried out starting from the equation for the sound field P' in inhomogeneous moving medium, as shown by Ostashev et al. [137]. With the assumption of a uniform density, the equation reads

$$\left[\nabla^2 + k^2(1+\epsilon) - \frac{2i}{\omega}\frac{\partial v_i}{\partial x_j}\frac{\partial^2}{\partial x_i \partial x_j} + \frac{2ik}{c_o}\boldsymbol{v}\cdot\nabla\right]P'(r) = 0 \tag{27}$$

where = ω/c_0, ω is the radian frequency of the sound, c_0 is the reference speed of sound, $P'(r)$ is the monochromatic sound pressure field, and $\epsilon = (c_0/c)^2 - 1$. Note that Eq. (27) reduces to the Helmholtz equation if $\boldsymbol{v} = 0$, i.e. without ambient flow. More details of the mathematical manipulations in order to reduce the equation to a one-way parabolic equation are referred to Ostashev et al. [137].

The derived equations can be solved with various numerical techniques. The WindSTAR-Pro package is developed with multiple options, either using finite difference methods or FFP (Fast Field Program) such as CNPE (Crank-Nicholson Parabolic Equation, see Salomons [67]) and GFPE (Green's Function Parabolic Equation, see Gilbert [138]). Depending on the PE method that is selected, the treatment of the undulating terrain may vary. Two different methods are implemented, namely domain decomposition or terrain following coordinates. In the first method, one treats the complex terrain as a succession of flat domains. After each flat domain, the coordinate system (x, z) is rotated so that the x-axis remains parallel to the ground, see Aballéa [139]. The second method is based on terrain following coordinate transformation

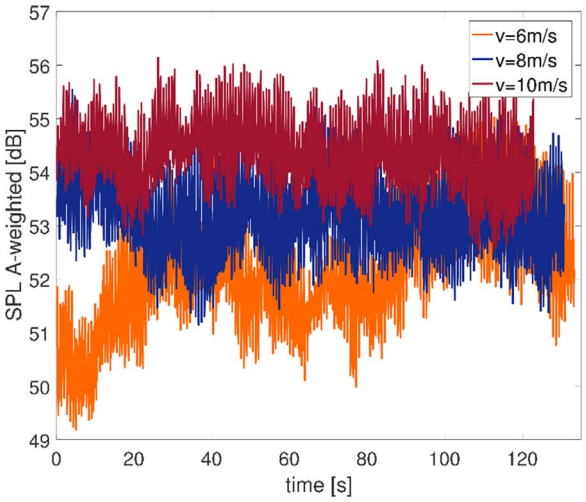

Fig. 17. A-weighted overall sound pressure levels for wind speeds of v = 6, 8, 10 m/s over a short time period.

of the Helmholtz equation followed by Sack and West [140]. Different PE methods that are implemented in the solver are summarized in Table 2:

In addition to the terrain geometry, all these PE methods require a set of noise source and flow inputs. These inputs can be obtained from different methods that vary in computational time depending on the complexity and accuracy. These include simple or complex source models, simple analytical flow models, low or high fidelity flow solvers

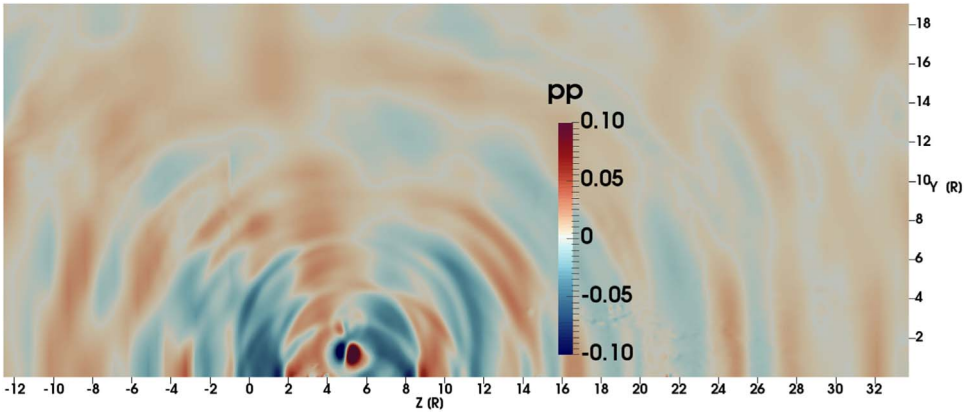

Fig. 16. Acoustic pressure at a wind speed of 10 m/s for a turbine placed at Z = 5 R and Y = 1.8 R.

Table 2
List of the numerical methods for wind turbine noise propagations developed at DTU.

PE methods	Velocity treatment	Terrain treatment	Numerical technique	Required resolution (1/lambda)	Additional note
Wide Angle (WAPE)	Scalar	Domain Decomposition	Finite Diff.	$\frac{\lambda}{8}-\frac{\lambda}{10}$	Tridiagonal Solver
Mean-Wind (MW-WAPE)	Vector	Domain Decomposition.	Finite Diff.	$\frac{\lambda}{8}-\frac{\lambda}{10}$	Penta-diagonal Solver
Turbulent-Wind (TW-WAPE)	Vector	Domain Decomposition	Finite Diff.	$\frac{\lambda}{8}-\frac{\lambda}{10}$	Penta-diagonal Solver
Green's Function (GFPE)	Scalar	Domain Decomposition.	FFTs	$5\lambda - 40\lambda$	Not relevant
Generalized Terrain (GTPE)	Scalar	Terrain Follow	Finite Diff.	$\frac{\lambda}{8}-\frac{\lambda}{10}$	Tridiagonal Solver

or field experiments. The source models and flow inputs are listed below:

1. **Starter function:** a starter function is always needed to begin the PE calculation. The initial SPL values from a wind turbine are desired such that this function mimics wind turbine as a sound source as accurately as possible.

(a) *Single point source*
This is the conventional approach for a steady single point source representing a monopole as the PE starting function. An adjustment for capturing wind turbine far field directivity [31] can be carried out by weighting the starter function with a source strength obtained at the observer azimuthal angle. This results in a similar sound pressure field shown in Fig. 18. This approach applies a relatively simpler monopole sound source and combines with wind turbine noise directivity characteristics.

(a) *Moving source along the rotor*
A more realistic source approach can be achieved by taking into account blade rotating phenomena. The unsteady dynamic nature of a wind turbine as a sound source is taken into account by the moving source approach. Wind turbine aerodynamic noise is mainly located in the outer part of a blade, such that a wind turbine can be treated as lumped sources located near the blade tips. Therefore, different source locations result in dynamic sound pressure level changes as well as in sound directivity changes. The idea behind this approach is to reduce the complex 3D source to three incoherent sources rotating with the blades. In this approach, only a specific time step corresponding to the true blade position in the vertical line can be used. A more consistent moving source approach should be added where a number of rotational azimuth angles and corresponding 2D plans are selected. As shown in Fig. 19, in such case, a wind turbine that is rotating in and out of the 2D PE plane intersects the domain at the bottom and the top tip heights. Thus we model it via a point source that is translated either up or down at each time step taking the turbine rotational speed into account.

(a) *Coupling with an unsteady source model*
A more sophisticated and computationally demanding model is to couple the PE model with a time varying sound source model. Each of the wind turbine noise generation models that are elaborated in the previous sections can be coupled with PE. With this approach the source power level at each time step is extracted from a noise generation model (for example, the BPM model) and then fed into PE for accurate propagation calculations. Repeating this multiple time steps yields a more realistic wind turbine noise time signal in the far field. Due to the large computational effort, this approach is not yet extensively used, however it is a more promising method for capturing the unsteadiness of both source and propagation phenomena.

2. **Background flow field**: as aforementioned, the conventional approach uses a combined value for speed of sound and wind speed. For this we need the temperature distribution as well as the wind field that is projected onto the PE 2D plans from source to receiver. These are obtained from:
   (a) 'Monin Obukhov Similarity Theory' + 'Analytical Wake Model'. The idea is based on the superposition of an atmospheric wind profile with an analytical wake model.
   (b) 'Linearized Flow Solver' + 'Analytical Wake Model': The background flow field is obtained from a linearized flow solver (for example, the WAsP Engineering software developed at DTU). Since the turbine effect is not modeled with the flow solver, the superposition with an analytical wake model is carried out. Additionally, synthetically generated turbulence is superimposed.
   (c) 'Reynolds averaged NS (RANS)' + 'Actuator Disc (AD): The EllipSys3D solver using Reynolds Averaged NS equations where the turbine is modeled with an Actuator Disc method [141–143] is used. In this approach, the initial background flow and turbine generated wake are simulated together.
   (d) 'LES' + 'AL': The EllipSys3D solver using Large Eddy Simulation where the turbine is modeled with an Actuator Line technique is used. This yields a time dependent flow output, thereby at each time step the background flow for PE is updated. This is so far the most accurate and time consuming method.
   (e) Field flow measurements from a single or multiple met masts or a lidar: This method is reserved for code validations.
3. **Ground impedance**: The ground characteristics are needed to determine the boundary conditions for PE.
   (a) Model of Delany and Bazley [144]: An empirical model for the calculation of ground impedance, obtained from fibrous absorbing materials.
   (b) Model of Attenborough [145]: Theoretical model for the calculation of ground impedance where, the ground is approximated as a semi-infinite porous medium, or as a porous layer with a rigid backing.

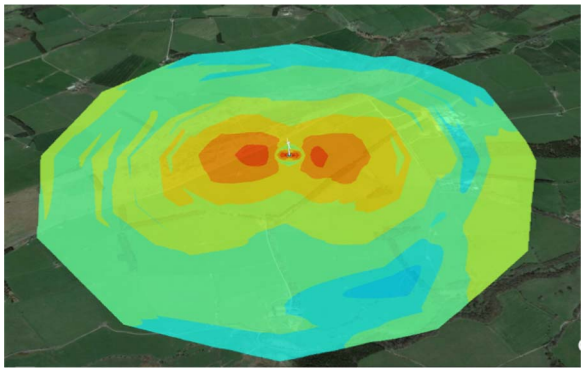

Fig. 18. Example of wind turbine noise modeled with a single point source at hub height.

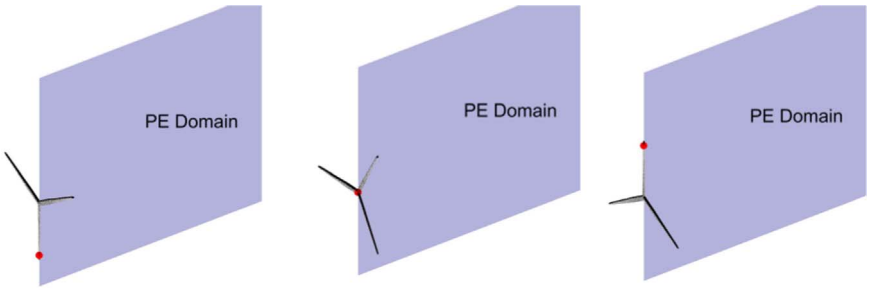

Fig. 19. Snapshots of source locations during a rotation.

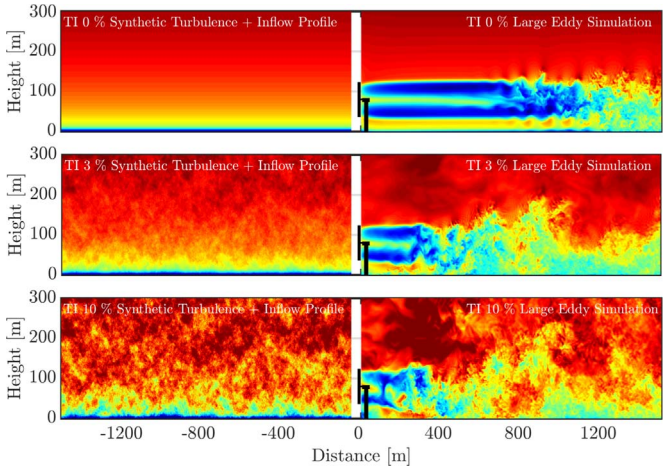

Fig. 20. Ambient flow and wake behind a single wind turbine.

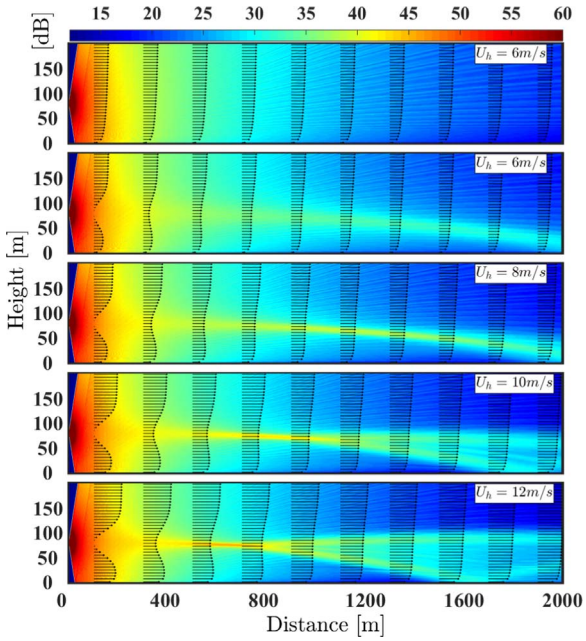

Fig. 21. SPL at a hub-height wind speed of 6 m/s without wake effects (upper figure) and with wake effects, and wind speeds of 8 m/s, 10 m/s, 12 m/s with wake effects [133].

4.2. Wind turbine noise propagation modeling

Using various combinations of the PE inputs, the single wind turbine noise propagation on flat terrain is studied extensively by the authors [131–133]. In these studies, the effects of wind shear, turbulence levels and source modeling techniques are investigated. The simulated wind turbine wake under different Turbulence Intensity (TI) is seen in Fig. 20. The inflow turbulence intensity clearly influences the wake structure, which further affects the sound propagation in the wake.

To investigate the influence from wind turbine wake, PE simulations are carried out at 6 m/s inflow wind speed under neutral atmospheric stability condition. In Fig. 21, the horizontal wind speed is shown as vectors and the color graphs are the sound pressure level generated from a wind turbine at a hub height of 80 m. The differences in SPL are clearly seen for the cases with and without wake effect. Including the effect of wake, the wind turbine noise propagation is also influenced by the incoming wind speeds, as shown in Fig. 21. The effect of varying wind speeds is mainly due to the change of the wake profile that reflects sound waves in different directions.

Considering a receiver located at 2 m' height above the ground level, we may have a close look at the sound pressure loss along the fixed propagation path. In Fig. 22, the change of SPL along a distance about 2500 m is shown. For the case at a wind speed of 10 m/s without wake effects, the line with triangles indicates a simple logarithmic decay of SPL. The other three cases show the sound propagation under the effects of wind turbine wakes at the three wind speeds. For these three cases, it is observed that there is an increase of SPL up to 12 dB compared to the case without wake effects. From such study, it is realized that the wind turbine noise propagation is strongly affected by the wake itself. Using the logarithmic decay for wind turbine sound propagations is not a good assumption.

Other effects, such as wind shear, also play important roles. Fig. 23 contains the information of TI and wind shear effects. The SPL contours clearly show that increasing TI and shear factor leads to different SPL distributions. As shown in the figure, the computational domain also includes the sound propagation in the upstream direction. The wind turbine rotor center is located at $x = 0$ m and $z = 80$ m. The wind comes from left to right such that the sound waves in the upstream direction are bended upwards. On the right hand side, the sound wave propagates towards the ground level that might create a noise problem to the receiver. As plotted in the figure, on each row there is an increase of wind shear from 0.14 to 0.45 and on each column the turbulence intensity increases from 0% to 10%. Thus, the plot shows a matrix of wind shear and turbulence effects. In such a study, it is seen that the inflow turbulence level is an important factor for wind turbine noise propagations in the downstream direction. In the upstream direction, the effect from wind shear is more evident. In general, the noise level upstream is lower than in downstream, but it is not necessarily true in the near field and a few diameters away from the rotor.

As a summary of the wind turbine noise propagation study, the influence of atmospheric condition for wind turbine noise propagation is listed below:

(a) Sound waves go through local upward and downward refracting regions, as a result of the wake deficit behind a wind turbine. This means that acoustic simulations without the wake cannot properly estimate the far field noise. The main parameter is the persistence of the wake, particularly in stable atmospheric conditions where the wake is long, and considerably a high SPL amplification is observed in the far field.

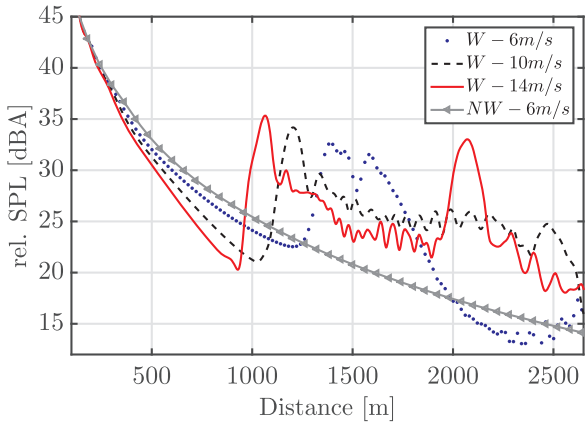

Fig. 22. SPL received at 2-meter height above the ground along the distance over 2500 m in a neutral atmospheric boundary layer. Cases with wake (W) and without wake (NW) [133].

(b) Far field (above 900 m) noise levels for upwind propagations are much lower than in the downwind case. However, it was also observed that at certain near field distances (200–500 m) the levels of the upwind propagations were higher than in the downwind case. This underlines the fact that the downwind propagation is not necessarily the worst case scenario for an elevated source, as e.g. a wind turbine.

(c) Comparisons of the two different source modeling techniques (moving and steady) coupled with LES concluded that the effect of source movement in the far field (beyond 700 m) diminishes with increasing incoming turbulence intensity. On the other hand, at the near field the effect of the moving source is always felt. The standard deviation values of SPL with steady and moving sources collapses to about 10% after 140 m, and to approximately 3% after 180 m.

(d) The higher ambient turbulence intensity results in increased sound source power levels, particularly in the low frequency domain (31.5–300 Hz). This directly affects the far field noise spectrum (up to a distance of 2500 m), as the atmospheric absorption is negligible in this frequency range.

(e) The time-dependent SPL analysis (obtained by running PE simulations successively with updated flow fields) showed that the SPL modulation close to the turbine (up to 250 m) has a similar behavior under all the flow conditions. It is also important to underline that in these regions the high frequency content of the source power level is just as important as the low frequency one. As the propagation distance increases, the turbulence and wind shear effects become more important. For upwind propagations, increasing turbulence results in a less modulation depth, because of the scattered waves to the shadow zones. For downwind propagations, dependent on the distance from the source, the wind shear and turbulence intensity either increase or decrease the modulation depth. It is not easy to conclude the trend; however, we observed clearly that these two factors are important for the far field amplitude modulation.

(f) Further investigations of the SPL modulation due to wake deficits showed that particularly the low incoming turbulence level (0% and 3%) results in an increased spectral energy of the low acoustic frequency content over wide spread propagation distances. This can lead to beating noise in the farfield.

5. Conclusions

In this paper, wind turbine noise generation and propagation models developed at DTU are presented and summarized, with a focus mainly on the numerical modeling. The applications of the models depend on the available computational resources, and the purpose of study. The NS-based CAA methods are computationally heavy and mainly suitable for understanding detailed noise generation mechanisms. The engineering oriented models are more applicable for airfoil and rotor design purposes because of the requirement of little computational effort. Wind turbine noise generation models can be coupled with wind turbine noise propagation models, such that a complete wind turbine noise simulation tool is developed. In the past, as compared to the research on wind turbine noise generation, there has been less focus on long distance wind turbine noise propagation problems, especially in connection with turbulent inflow, turbulent wake, and wind shear. It is found that the atmospheric flow conditions can be well coupled to the PE method. The simulations showed that wind turbine noise propagation is largely influenced by the ambient flow, as well as by the wake created by the wind turbine. The PE model can be naturally coupled with a CFD generated flow-field to simulate the wind turbine noise propagation through complex terrain and complex atmospheric conditions.

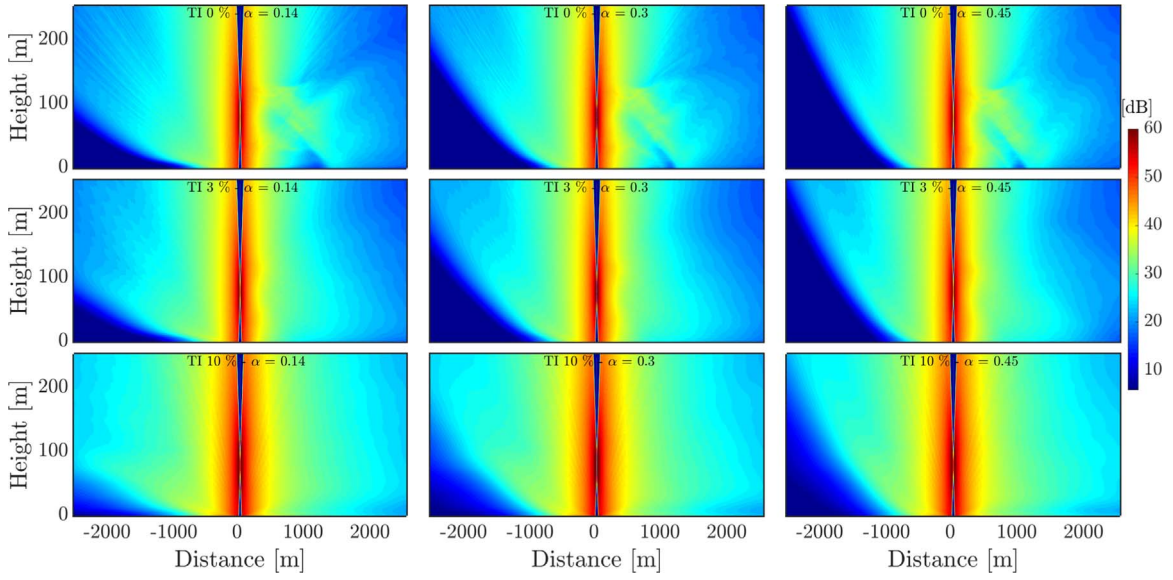

Fig. 23. Time-averaged SPL under various flow conditions. Source is located at 0 m distance; flow comes from left to right. From top to bottom: turbulence intensity is 0%, 3% and 10%; From left to right: the wind shear factor is 0.14, 0.3 and 0.45.

Acknowledgement

This work is supported by the Chinese National Nature Science Foundation under Grant no. 11672261. Thanks everyone who has contributed to this article for providing figures and proof-reading.

References

[1] Søndergaard B. Noise and low frequency noise from wind turbines. In: Inter. noise 2014. Melbourne, Australia; 2014, p. 1–12.
[2] Lighthill MJ. On sound generated aerodynamically: I. General theory. Proc R Soc Lond Ser A 1952;211:564.
[3] Curle N. The influence of solid boundaries upon aerodynamic sound. Proc R Soc Lond Ser A 1955;231:505–14.
[4] Ffowcs Williams JE, Hall LH. Aerodynamic sound generation by turbulent flow in the vicinity of a scattering half plane. J Fluid Mech 1970;40:657–70.
[5] Ffowcs Williams JE, Hawkings DL. Sound generation by turbulence and surfaces in arbitrary motion. Proc R Soc Lond Ser A 1969;264:321–42.
[6] Farassat F. Derivation of formulations 1 and 1A of Farassat [NASA/TM-2007-214853]. 2007.
[7] Farassat F, Casper J. Broadband noise prediction when turbulence simulation is available -derivation of formulation 2B and its statistical analysis. J Sound Vib 2012;331(10):2203–8.
[8] Hardin JC, Pope DS. An acoustic/viscous splitting technique for computational aeroacoustics. Theor Comput Fluid Dyn 1994;6:323–40.
[9] Shen WZ, Sørensen JN. Comment on the aeroacoustic formulation of Hardin and Pope. AIAA J 1999;1:141–3.
[10] Seo JH, Moon YJ. Perturbed compressible equations for aeroacoustic noise prediction at low Mach numbers. AIAA J 2005;43:1716–24.
[11] Ewert R, Schröder W. Acoustic perturbation equations based on flow decomposition via source filtering. J Comput Phys 2003;188:365–98.
[12] Shen WZ, Sørensen JN. Acoustic modelling of low-speed flows. Theor Comput Fluid Dyn 1999;13:271–89.
[13] Shen WZ, Sørensen JN. Aero-acoustic modelling of turbulent airfoil flows. AIAA J 2001;39:1057–64.
[14] Shen WZ, Sørensen JN. A collocated grid finite volume method for aeroacoustic computations of low-speed flow. J Comput Phys 2004;196:348–66.
[15] Shen WZ, Zhu WJ, Sørensen JN. Aero-acoustic computations for turbulent airfoil flows. AIAA J 2009;47:1518–27.
[16] Zhu WJ. Aero-acoustic computations of wind turbines [Technical Report, MEK-PHD 2007-09]. Lyngby: Institute for Mechanics, Energy and Construction, Danish Technical University; 2008.
[17] Zhu WJ, Shen WZ, Sørensen JN. High-order numerical simulations of flow induced noise. Int J Numer Methods Fluids 2011;66:17–37.
[18] Tam C, Webb J. Dispersion-relation-preserving finite difference schemes for computational acoustics. J Comput Phys 1993;107:262–81.
[19] Bailly C, Lafon P, Candel S. A stochastic approach to compute noise generation and radiation of free turbulent flows. AIAA Pap 1995:092.
[20] Bailly C, Juv´e D. A stochastic approach to compute subsonic noise using linearized Euler's equations. AIAA Pap 1999&;;1872.
[21] Bogey C, Bailly C, Juvé D. Computation of flow noise using source terms in linearized Euler's equations. AIAA J 2002;40:235–43.
[22] Amiet RK. Acoustic radiation from an airfoil in a turbulent stream. J Sound Vib 1975;41(4):407–20.
[23] Amiet RK. Noise due to turbulent flow past a trailing edge. J Sound Vib 1976;47(3):387–93.
[24] Viterna LA. The NASA LeRC wind turbine sound prediction code [NASA CP-2185]. 1981. p. 410–8.
[25] Bareiß R, Guidati G, Wagner S. An approach towards refined noise prediction of wind turbines. In: Tsipouridis JL, editor. Proceedings of the European wind energy association. Conference & exhibition, Vol. 1. Thessaloniki; 1984, p. 785–90.
[26] Glegg SAL, Baxter SM, Glendinning AG. The prediction of broadband noise from wind turbines. J Sound Vib 1986;118:217–39.
[27] De Wolf WB. EN Predictiemethod Voor Her Aerodynamische Geluid Van Winddurbines Met Horizontale AS [NLR TR 87018 L]. 1986. p. 1–55.
[28] Grosveld FW. Prediction of broadband noise from horizontal axis wind turbines. J Propuls Power 1985;1:292–9.
[29] Lowson MW. Assessment and prediction of wind turbine noise. 1. Basic aerodynamic and acoustic models [Flow solutions report 1993/06, W/13/00317/00/00]. 1993. p. 1–46.
[30] Brooks TF, Pope DS, Marcolini MA. Airfoil self-noise and prediction. USA: NASA Reference Publication 1218, National Aeronautics and Space Administration; 1989.
[31] Zhu WJ, Heilskov N, Shen WZ, Sørensen JN. Modeling of aerodynamically generated noise from wind turbines. J Sol Energy Eng 2005;127:517–28.
[32] Leloudas G, Zhu WJ, Shen WZ, Sørensen JN, Hjort S. Prediction and reduction of noise from a 2.3 MW wind turbine. The science of making torque from wind. J Phys: Conf Ser 2007;75:012083.
[33] Zhu WJ, Shen WZ, Sørensen JN, Leloudas G. Improvement of airfoil trailing edge bluntness noise model. Adv Mech Eng 2016;8(2):1–12. http://dx.doi.org/10.1177/1687814016629343.
[34] NWTC Information Portal (NAFNoise). ⟨https://nwtc.nrel.gov/NAFNoise⟩, [Accessed 27 August 2017].
[35] Madsen HA. Low frequency noise from wind turbines mechanisms of generation and its modelling. J Low Free Noise Vib Act Cont 2010;29(4):239–51.
[36] Bertagnolio F, Madsen HA, Christian B, Niels T, Fischer A. Aerodynamic noise characterization of a full-scale wind turbine through high-frequency surface pressure measurements. Int J Aeroacoustics 2015;14(5):729–66.
[37] Fischer A, Madsen HA, Bertagnolio F. Experimental investigation of the surface pressure field for prediction of trailing edge noise of wind turbine aerofoils. Int J Aeroacoustics 2015;14(6):767–809.
[38] Fischer A. Experimental characterization of airfoil boundary layers for improvement of aeroacoustic and aerodynamic modeling [Ph.D. Thesis]. Denmark: Technical University of Denmark; 2011.
[39] Wagner S, Bareiss R, Guidati G. Wind turbine noise. Berlin, Heidelberg: Springer; 1996.
[40] Lutz T, Arnold B, Wolf A, Krämer E. Numerical studies on a rotor with distributed suction for noise reduction. J Phys: Conf Ser 2014;524(1):012122. http://dx.doi.org/10.1088/1742-6596/524/1/012122.
[41] Wolf A, Lutz T, Würz W, Krämer E, Stalnov O, Seifert A. Trailing edge noise reduction of wind turbine blades by active flow control. J Wind Eng 2014;18(5):909–23. http://dx.doi.org/10.1002/we.1737.
[42] Herr M, Dobrzynski W. Experimental investigations in low-noise trailing-edge design. AIAA J 2005;43(6):1167–75.
[43] Finez A, Jondeau E, Roger M, Jacob MC. Broadband noise reduction with trailing edge brushes. AIAA Pap 2010:3980.
[44] Finez A, Jacob M, Jondeau E, Roger M. Broadband noise reduction with trailing edge brushes. In: Proceedings of the 16th AIAA/CEAS aeroacoustics conference, aeroacoustics conferences 2010. AIAA; 2010, 3980. ⟨http://dx.doi.org/10.2514/6.2010-3980⟩.
[45] Howe MS. A review of the theory of trailing edge noise. J Sound Vib 1978;61(3):437–65.
[46] Howe MS. Noise produced by a sawtooth trailing edge. J Acoust Soc Am 1991;90(1):482–7.
[47] Braun KA, van der Borg NJCM, Dassen AGM, Doorenspleet F, Gordner A, Ocker J, et al. Serrated trailing edge noise. In: Proceedings of the EU wind energy conference; 1999.
[48] Chong TP, Joseph PF. An experimental study of airfoil instability tonal noise with trailing edge serrations. J Sound Vib 2013;332(24):6335–58.
[49] Oerlemans S, Fisher M, Maeder T, Kögler K. Reduction of wind turbine noise using optimized airfoils and trailing edge serrations. AIAA J 2009;47(6):1470–81.
[50] Oerlemans S. Reduction of wind turbine noise using blade trailing edge devices. In: Proceedings of the 22nd AIAA/CEAS aeroacoustics conference, aeroacoustics conferences 2016. AIAA; 2016, 3018. ⟨http://dx.doi.org/10.2514/6.2016-3018⟩.
[51] Geyer T, Sarradj E, Fritzsche C. Measurement of the noise generation at the trailing edge of porous airfoils. Exp Fluids 2010;48:291–308.
[52] Jaworski JW, Peake N. Aerodynamic noise from a poroelastic edge with implications for the silent flight of owls. J Fluid Mech 2013;723:456–79. http://dx.doi.org/10.1017/jfm.2013.139.
[53] Katinas V, Marčiukaitis M, Tamašauskienė M. Analysis of the wind turbine noise emissions and impact on the environment. Ren Sus Energy Rev 2016;58:825–31.
[54] Thorne Bob. Wind farm noise and human perception – a review. Australia: Noise Measurement Services; 2013.
[55] Katsaprakakis DAl. A review of the environmental and human impacts from wind parks. A case study for the Prefecture of Lasithi, Crete. Renew Sustain Energy Rev 2012;16:2850–63.
[56] Enevoldsen P, Sovacool BK. Examining the social acceptance of wind energy: practical guide lines for on shore wind project development in France. Renew Sustain Energy Rev 2016;53:178–84.
[57] Huesca-Pérez ME, Sheinbaum-Pardo C, Köppel J. Social implications of siting wind energy in a disadvantaged region – the case of the Isthmus of Tehuantepec, Mexico. Renew Sustain Energy Rev 2016;58:952–65.
[58] John MP, Spyros GV. Noise propagation issues in wind energy applications. J Sol Energy Eng 2005;127:234–41.
[59] Pen Y, Zhou N, Chen J, Li KM. Propagation of wind turbine noise through the turbulent atmosphere. J Acoust Soc Am 2014;136:2205.
[60] Johansson L. Sound propagation around off-shore wind turbines [Licentiate Thesis, ISRN-KTH-BYT-/R-03/192-SE]. ISSN 1651-5536. Stockholm; 2003.
[61] Boué M. Long-range sound propagation over the sea with application to wind turbine noise. Final report for the Swedish Energy Agency project 21597-3 (trans) [TRITA-AVE 2007]. 2007. [22:ISSN 1651-7660].
[62] Forssén J, Schiff M, Pedersen E, Waye KP. Wind turbine noise propagation over flat ground: measurements and predictions. Acta Acust U Acust 2010;96:753–60.
[63] Cheng R, Morris P, Brentner K A 3D parabolic equation method for sound propagation in moving inhomogeneous media. In: Proceedings of the 13th AIAA/CEAS aeroacoustics conference.
[64] Zhu WJ, Sørensen JN, Shen WZ. An aerodynamic noise propagation model for wind turbines. Wind Eng 2005;29(2):129–43.
[65] Heimann D, Kaasler Y, Gross G. The wake of a wind turbine and its influence on sound propagation. Meteorol Z 2011;20:449–60.
[66] Lee S, Lee D, Honho S Prediction of far-field wind turbine noise propagation with parabolic equation. In: Proceedings of the 21st AIAA/CEAS aeroacoustics conference. Dallas, Texas; 2015.
[67] Salomons EM. Computational atmospheric acoustics. Netherlands: Springer Science Business Media B. V.; 2001.
[68] Ta Phuoc L. Modèles de Sous Maille Appliqués aux Ecoulements Instationnaires Décollés. In: Proceedings of the DRET conference: Aérodynamique Instationnaire Turbulente-Aspects Numériques et Expérimentaux. Paris, France: DGA/DRET editors; 1994.

[69] Bardina J, Ferziger JH, Reynolds WC. Improved subgrid scale models for large eddy simulation. AIAA Pap 1980;80:1357.
[70] Sagaut P. Large eddy simulation for incompressible flows. Third edition France: Springer; 2006.
[71] Michelsen JA. Basis3D – a platform for development of multiblock PDE solvers [Technical Report, AFM 92-05]. Denmark: Technical University of Denmark; 1992.
[72] Sørensen NN. General purpose flow solver applied to flow over hills [Risø-R-827-(EN)]. Roskilde, Denmark: Risø National Laboratory; 1995.
[73] Shen WZ, Michelsen JA, Sørensen JN. An improved Rhie-Chow interpolation for unsteady flow computations. AIAA J 2001;39:2406–9.
[74] Shen WZ, Michelsen JA, Sørensen NN, Sørensen JN. An improved SIMPLEC method on collocated grids for steady and unsteady flow computations. Numer Heat Trans Part B 2003;43:221–39.
[75] Smagorinsky J. General circulation experiments with the primitive equations. Mon Weather Rev 1963;91:99–164.
[76] Lilly DK. The representation of small-scale turbulence in numerical simulation experiments. Proc IBM Sci Comput Symp Environ Sci 1967:195–210.
[77] Deardorff JW. A numerical study of three-dimensional turbulent channel flow at large Reynolds numbers. J Fluid Mech 1970;41:453–80.
[78] Mary I, Sagaut P. Large eddy simulation of flow around an airfoil near stall. AIAA J 2002;40(6):1139–45.
[79] Piomelli U, Balaras E. Wall-layer models for large-eddy simulations. Annu Rev Fluid Mech 2002;34:349–74.
[80] Zhu WJ, Shen WZ, Bertagnolio F, Sørensen JN. Comparisons between LES and wind tunnel hot-wire measurements of a NACA 0015 airfoil. In: Proceedings of EWEA 2012 – European wind energy conference & exhibition; 2012, p. 975–82.
[81] Cavar D, Meyer KE. Investigation of turbulent boundary layer flow over 2D bump using highly resolved large eddy simulation. J Fluids Eng 2011;133:11. http://dx.doi.org/10.1115/1.4005262.
[82] Cavar D, Meyer KE. LES of turbulent jet in cross-flow: Part 1 – a numerical validation study. Int J Heat Fluid Flow 2012;36:18–34. http://dx.doi.org/10.1016/j.ijheatfluidflow.2011.12.009.
[83] Cavar D, Meyer KE. LES of turbulent jet in cross flow: Part 2 – POD analysis and identification of coherent structures. Int J Heat Fluid Flow 2012;36:35–46. http://dx.doi.org/10.1016/j.ijheatfluidflow.2012.03.010.
[84] Shen WZ, Zhu WJ, Sørensen JN. Actuator line/Navier–Stokes computations for the MEXICO rotor: comparison with detailed measurements. Wind Energy 2012;15(5):811–25.
[85] Shen WZ, Zhu WJ, Yang H. Validation of the actuator line model for simulating flows past yawed wind turbine rotors. J Power Energy Eng 2015;3:7–13.
[86] Troldborg N, Sørensen JN, Mikkelsen RF, Sørensen NN. A simple atmospheric boundary layer model applied to large eddy simulations of wind turbine wakes. Wind Energy 2014;17(4):657–69. http://dx.doi.org/10.1002/we.1608.
[87] Sheldahl RE, Klimas PC. Aerodynamic characteristics of seven airfoil sections through 180° angle of attack for use in aerodynamic analysis of vertical axis wind turbines [SAND80-2114]. Albuquerque, New Mexico, USA: Sandia National Laboratories; 1981.
[88] Marsden O, Bogey C, Bailly C. Noise radiated by a high-Reynolds-number 3-D airfoil. AIAA Pap 2005:2817.
[89] Wang M, Freund JB, Lele SK. Computational prediction of flow-generated sound. Annu Rev Fluid Mech 2006;38:483–512.
[90] Sandberg RD. Compressible-flow DNS with application to airfoil noise. Flow Turbul Combus 2015;95(2):211–29.
[91] Kim T, Lee S. Aeroacoustic simulations of a blunt trailing-edge wind turbine airfoil. J Mech Sci Technol 2014;28(4):1241–9.
[92] Kim JW, Haeri S, Joseph PF. On the reduction of aerofoil–turbulence interaction noise associated with wavy leading edges. J Fluid Mech 2016;792:526–50.
[93] Bogey C, Bailly C. A family of low dispersion and low dissipative explicit schemes for flow and noise computations. J Comput Phys 2004;194:194–214.
[94] Cunha G, Redonnet S. On the effective accuracy of spectral-like optimized finite-difference schemes for computational aeroacoustics. J Comput Phys 2014;263:222–32.
[95] Zhuang M, Chen RF. Optimized upwind dispersion-relation preserving finite difference scheme for computational aeroacoustics. AIAA J 1998;36:2146–8.
[96] Zhuang M, Chen RF. Applications of high-order optimized upwind schemes for computational aeroacoustics. AIAA J 2002;40:443–6.
[97] Berland J, Bogey C, Bailly C. Optimized explicit schemes: matching and boundary schemes and 4th-order Runge-Kutta algorithm. AIAA Pap 2004:2814.
[98] Lele SK. Compact finite difference schemes with spectral-like resolution. J Comput Phys 1992;103:16–42.
[99] Kim JW, Lee DJ. Optimized compact finite difference schemes with maximum resolution. AIAA J 1996;34:887–93.
[100] Visbal MR, Gaitonde DV. Very high-order spatially implicit schemes for computational acoustics on curvilinear meshes. J Comput Acoust 2001;9:1259–86.
[101] Kim JW. Optimised boundary compact finite difference schemes for computational aeroacoustics. J Comput Phys 2007;225:995–1019.
[102] Carpenter MH, Gottlieb D, Abarbanel S. The stability of numerical boundary treatments for compact high-order finite-difference schemes. J Comput Phys 1993;108:272–95.
[103] Arbey H, Bataille J. Noise generated by airfoil profiles placed in a uniform laminar flow. J Fluid Mech 1983;134:33–47.
[104] Nash EC, Lowson MV, McAlpine A. Boundary layer instability noise on aerofoils. J Fluid Mech 1999;382:27–61.
[105] Kingan MJ, Pearse JR. Laminar boundary layer instability noise produced by an aerofoil. J Sound Vib 2009;322(4):808–28.
[106] Cheng JT, Zhu WJ, Fischer A, Ramos GN, Madsen J, Chen J, et al. Design and validation of the high performance and low noise CQU-DTU-LN1 airfoils. Wind Energy 2014;17(12):1817–33.
[107] Zhu WJ, Shen WZ. LES tests on airfoil trailing edge serration. J Phys: Conf Ser 2016;753(3):022062.
[108] Zhu WJ, Shen WZ. Airfoil trailing edge noise generation and its surface pressure fluctuation. J Power Energy Eng 2015;3:14–9.
[109] Zhu WJ, Shen WZ. Numerical simulation of airfoil trailing edge serration noise. In: Proceedings of the 6th international meeting on wind turbine noise. Glasgow, UK; 2015.
[110] Amiet RK. Effect of the incident surface pressure field on noise due to turbulent flow past a trailing edge. J Sound Vib 1978;57:305–6.
[111] Roger M, Moreau S. Back-scattering correction and further extensions of Amiet's trailing edge noise model. J Sound Vib 2005;286(3):477–506.
[112] Goody M. Empirical spectral model of surface pressure fluctuations. AIAA J 2004;42(9):1788–94.
[113] Rozemberg Y, Robert G, Morreau S. Wall-pressure spectral model including the adverse pressure gradient effect. AIAA J 2012;50(10):2168–79.
[114] D'Amico S. Validation and improvement of a noise prediction model for wind turbines. Denmark: Thesis work at DTU Wind Energy; 2017. [M-0118].
[115] Tian Y. Modelling of wind turbine noise sources and propagation in the atmosphere. France: Thesis work at University Paris Saclay; 2015.
[116] Tian Y, Cotté B. Wind turbine noise modeling based on Amiet's theory: effects of wind shear and atmospheric turbulence. Acta Acust U Acust 2016;102(4):626–39.
[117] Madsen HA, Bertagnolio F, Fischer A, Bak C, Paulsen US. A novel full scale experimental characterization of wind turbine aero-acoustic noise sources – preliminary results. Hawaii: ISROMAC; 2016.
[118] Parchen R. Progress report DRAW: a prediction scheme for trailing-edge noise based on detailed boundary-layer characteristics [TNO report. HAGRPT-980023]. The Netherlands: TNO Insititute of Applied Physics; 1998.
[119] Fischer A. Experimental characterization of airfoil boundary layers for improvement of aeroacoustic and aerodynamic modeling [Ph.D. Thesis]. Roskilde, Denmark: DTU Wind Energy Department; 2011.
[120] Bertagnolio F, Fischer A, Zhu WJ. Tuning of turbulent boundary layer anisotropy for improved surface pressure and trailing-edge noise modelling. J Sound Vib 2014;333:991–1010.
[121] Fischer A, Bertagnolio F, Madsen HA. Improvement of TNO type trailing edge noise model. Eur J Mech – B/Fluids 2016;61:255–62.
[122] Bertagnolio F, Madsen HA, Fischer A, Bak C. Validation of an aero-acoustic wind turbine noise model using advanced noise source measurements of a 500 kW turbine. In: Proceedings of 16th international symposium on transport phenomena and dynamics of rotating machinery; 2016.
[123] Bertagnolio F, Madsen HA, Fischer A, Bak C. A semi-empirical airfoil stall noise model based on surface pressure measurements. J Sound Vib 2017;387:127–62.
[124] Bertagnolio F. Experimental investigation of stall noise towards its modelling. In: 6th international conference on wind turbine noise. Conference proceedings. Glasgow, UK; 2015.
[125] Larsen TJ, Hansen AM. HAWC2, the user's manual [Tech, Rep. RISØ-R-1597(ver.3-1)]. Roskilde, Denmark: Risø-DTU; 2017.
[126] Bertagnolio F, Madsen HA, Fischer A. A combined aeroelastic-aeroacoustic model for wind turbine noise: verification and analysis of field measurements. [online]. Wind Energy2017. http://dx.doi.org/10.1002/we.2096.
[127] Debertshäuser H, Shen WZ, Zhu WJ. Development of a high-fidelity noise prediction and propagation model for noise generated from wind turbines. In: Proceedings of the 6th international meeting on wind turbine noise. Glasgow, UK; 2015.
[128] Debertshäuser H, Shen WZ, Zhu WJ. Aeroacoustic calculations of wind turbine noise with the actuator line/Navier-Stokes technique. In: Proceedings of the 34th wind energy symposium. San Diego, CA: American Institute of Aeronautics & Astronautics; 2016.
[129] Sørensen JN, Shen WZ. Numerical computations of wind turbine wakes. J Fluids Eng 2002;124:393–9.
[130] Zhu WJ, Shen WZ, Sørensen JN. Wind turbines – design, control and applications. [ISBN 978-953-51-2496-2, Print ISBN 978-953-51-2495-5, 350 pages]. UK: InTech; 2016. http://dx.doi.org/10.5772/61672.
[131] Barlas E, Zhu WJ, Shen WZ, Andersen SJ. Wind turbine noise propagation modelling: an unsteady approach. The science of making torque from wind. [ISSN:1742-6596]. J Phys: Conf Ser 2016;753. http://dx.doi.org/10.1088/1742-6596/753/2/022003.
[132] Barlas E, Zhu WJ, Shen WZ, Dag K, Moriarty P. Investigation of amplitude modulation noise with a fully coupled wind turbine noise source and advanced propagation model. Int Conf Wind Turbine Noise 2017.
[133] Barlas E, Zhu WJ, Shen WZ, Sørensen JN, Kelly M, Andersen SJ. Effect of wind turbine wake on atmospheric sound propagation. Appl Acoust 2017;122:51–61.
[134] Bertagnolio F. A noise generation and propagation model for large wind farms. In: Proceedings of the 22nd international congress on acoustics; 2016. ICA2016-86.
[135] Berengier MC, Gauvreau B, Blanc-Benon Ph, Juve D. Outdoor sound propagation: a short review on analytical and numerical approaches. Acta Acust 2003;89:980–91.
[136] Blanc-Benon Ph, Dallois L, Juve D. Long range sound propagation in a turbulent atmosphere within the parabolic approximation. Acta Acust 2001;87:659–69.
[137] Ostashev V, Juve D, Blanc-Benon Ph. Derivation of a wide-angle parabolic equation for sound waves in inhomogeneous moving media. Acta Acust 1997;83(3):455–60.
[138] Gilbert KE. A numerically stable formulation of the Green's function parabolic equation: subtracting the surface-wave pole [Published Online]. JASA Express Lett2014.

[139] Aballéa F. Propagation acoustique en milieu extérieur: application de l'équation parabolique rapide au couplage d'effets météorologiques et de topographies complexes "Using the fast parabolic equation in complex topographies, including meteorological effects, for sound propagation outdoors" [Ph.D. Dissertation]. France: Université de Maine; 2004.
[140] Sack RA, West M. A parabolic equation for sound propagation in two dimensions over any smooth terrain profile: the generalised terrain parabolic equation (GT-PE). Appl Acoust 1995;45(2):113–29.
[141] Mikkelsen RF, Sørensen JN. Actuator disc methods applied to wind turbines [Ph.D. Thesis]. Technical University of Denmark; 2004. [Published].
[142] Tian LL, Zhu WJ, Shen WZ, Sørensen JN, Zhao N. Investigation of modified AD/RANS models for wind turbine wake predictions in large wind farm. J Phys: Conf Ser 2014;524(1).
[143] Sarmast S, Shen WZ, Zhu WJ, Mikkelsen RF, Breton SP, Ivanell S. Validation of the actuator line and disc techniques using the new MEXICO measurements. J Phys: Conf Ser 2016;753(3). http://dx.doi.org/10.1088/1742-6596/753/3/032026.
[144] Delany ME, Bazley EN. Acoustical properties of fibrous absorbent materials. Appl Acoust 1970;3:105–16.
[145] Attenborough K. Acoustical impedance models for outdoor ground surfaces. J Sound Vib 1985;99:521–44.